The information in this report is preliminary and may be supplemented or corrected.

BACKGROUND

On July 18, 2013, CSX train no. Q704-19, consisting of two locomotives and 24 loaded flat cars carrying municipal waste, derailed at milepost 9.99 on Metro-North's Hudson Division in the Bronx New York while traveling northbound towards Spuyten Duyvil station, Figure 1.

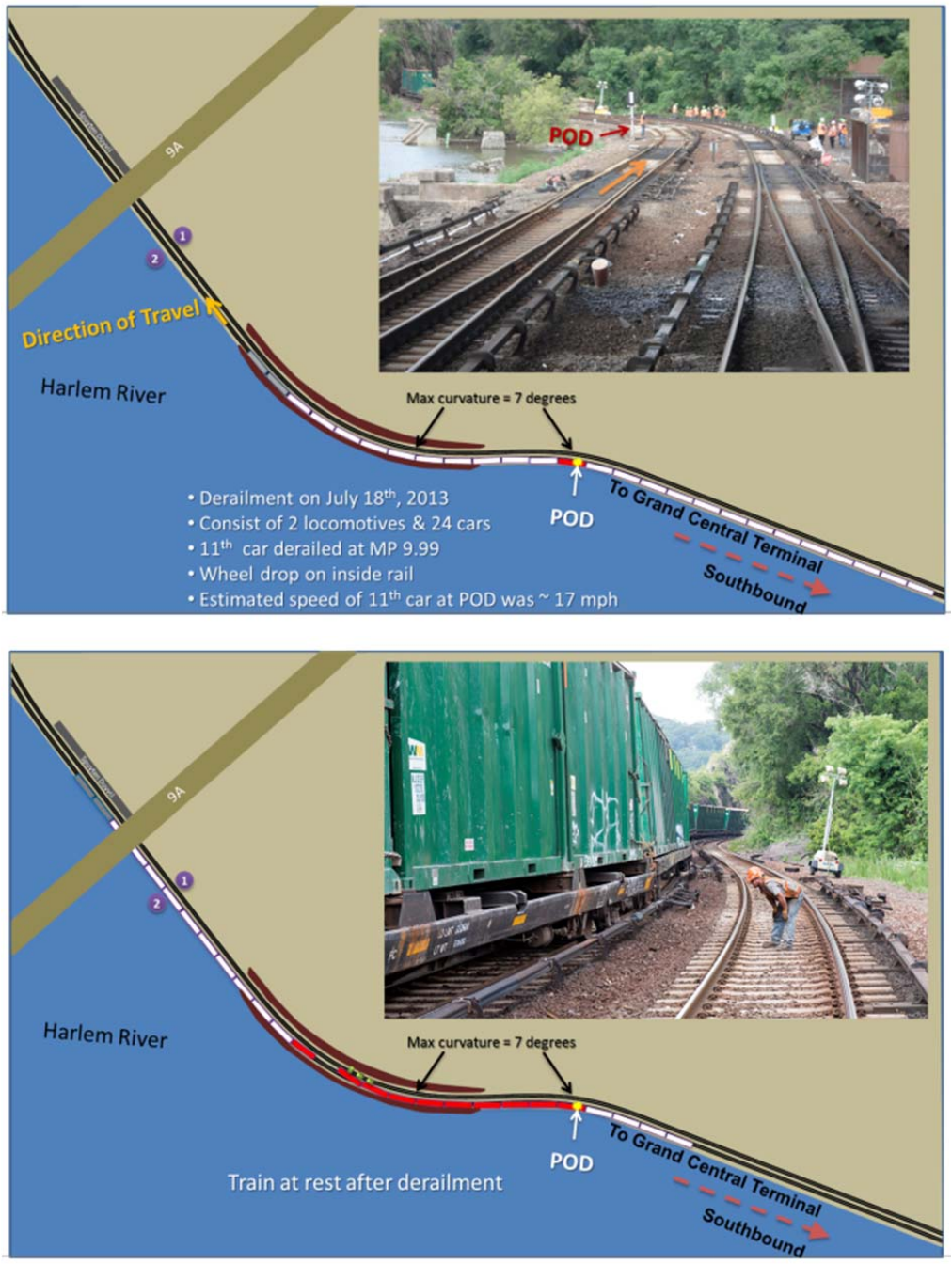

Figure 1: Sketch of derailment area: (1a, top) initial position of train no. Q704-19 when 11th car derailed; and, (1b, bottom) final position of train no. Q704-19 at rest following derailment, cars 11 – 20 derailed.

The Volpe National Transportations Systems Center (Volpe Center) was requested to provide engineering support to the National Transportation Safety Board (NTSB), the Federal Railroad Administration (FRA), and the investigation parties[1] with assessment of (1) wheel-rail interaction (wheel-rail forces, wheel-rail contact geometry, etc.), (2) the overall track condition (track geometry, etc.), and (3) the behavior of Metro-North crossties under load. This engineering support was based on the following data:

- Photographs;
- FRA DOTX220 Track Geometry Data recorded June 4th and June 19th 2013;
- Metro-North Track Geometry Data recorded April 2013;
- Track notes taken after the accident;
- Wheel and rail profile measurements;
- Car weight data;
- Examination of wheels at CSX's Selkirk Yard, Selkirk, NY;
- Examination of crossties at Metro-North's Highbridge Yard, Bronx, NY; and,
- Observation of crosstie testing at Wiss, Janney, Elstner Associates, Inc. (WJE) in Northbrook, IL.

The results of these efforts are documented below.

WHEEL-RAIL INTERACTION

Although ten cars of the 24 car train eventually derailed and came to rest at various locations throughout the reverse curve, car 11 was the first to derail as it was traveling northbound at approximately 17 mph through the left-hand curve shown in the Figure 2 photo. Based on matching of markings found on the low-rail with those on the wheels of car 11, it was determined that the low-rail wheel of its lead-truck-lead-axle dropped within the gage. The derailment scenario is illustrated in the Figure 2 sketch with the derailed wheel represented as the starred wheel. In general, a wheel dropping within the gage may result from one or more of a number of distinct causes (or derailment modes) such as wheel-climb (when a flanging wheel climbs onto the top of the railhead while the opposite, non-flanging wheel drops within the gage) or rail-rollover (complete outward rotation of one of the rails from its original position on top of the crosstie, resulting in wide-gage and wheel drop within the gage). Both of these derailment modes are related to the combined effect of the lateral and vertical dynamic loads generated at the wheel-rail interface, the latter involves structural failure of the track – i.e. the fasteners fail to maintain the proper gage. While physical evidence did not appear to support a wide-gage rail-rollover derailment (in particular, as the train continued forward the other wheels of the car traversed the area without derailing and/or riding on the web of a rolled rail as might be expected to occur in a rail-rollover derailment), other derailment modes were considered including a wide-gage scenario in which the rails momentarily spread apart just enough for derailment of a flanging axle, but not enough for derailment of a centered, non-flanging axle (if an axle remains centered, gage will have to spread beyond the width of both wheels rather than just one width as in the case of a flanging axle).

[1] The parties to the investigation were FRA; Metro-North Railroad (MN); CSX Railroad; Waste Management of New York; and Koppers Inc.

This wide-gage derailment scenario, described again in greater detail later, is probable if the orientation of a truck during curve negotiation results in flange contact on one axle and not on the other, a condition that depends upon a number of factors including axle spacing, curve radius, and cant deficiency. The sketch in Figure 2 illustrates the nominal tracking position of axles in a freight truck resulting from the normal orientation of a freight truck during negotiation of the relatively sharp curve present at the derailment at low cant deficiency. In this case, the lead axle offsets laterally from the track centerline to the point that flange contact on the high-rail is established and a large angle of attack is developed (resulting in increased risk of derailment) at the same time that the trailing axle of a truck tends to be centered between the rails with low angle of attack.

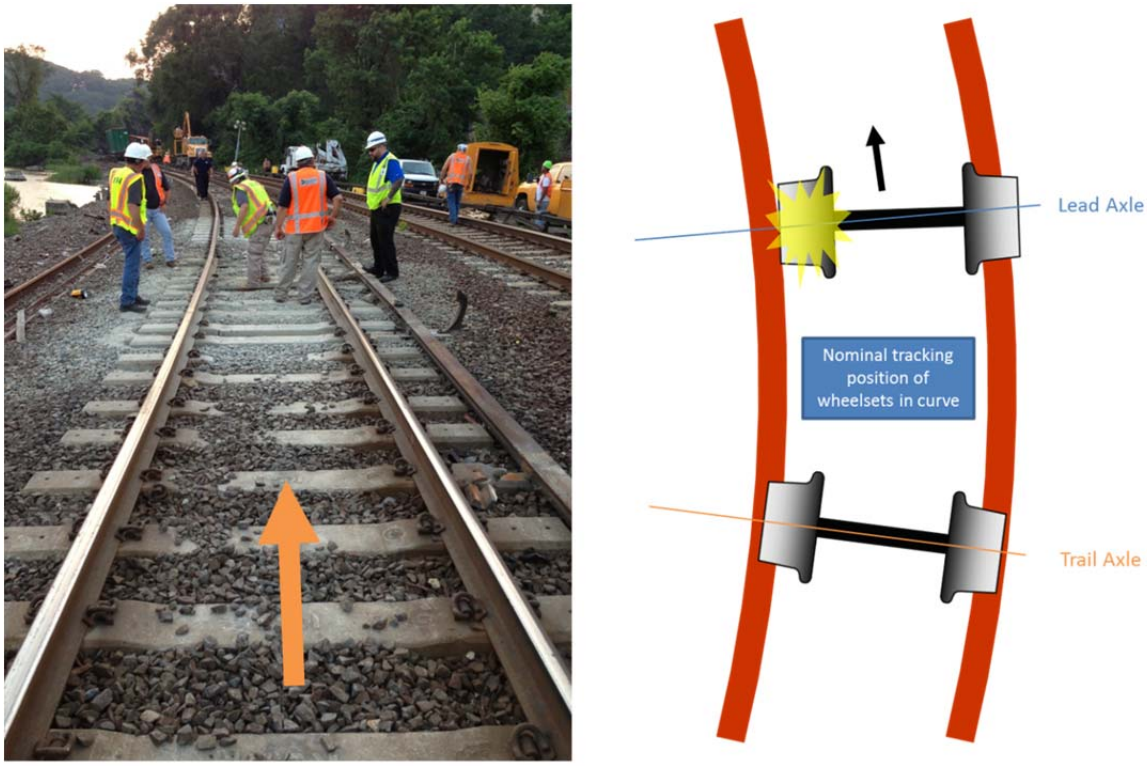

Figure 2: Car 11 low-rail wheel of lead-truck-lead-axle dropped within the gage while traveling northbound through left-hand curve at approximately 17 mph.

Vehicle-track interaction (VTI) simulations were conducted to estimate wheel-rail interaction forces that were likely present on car 11 during the derailment while negotiating the combination of track geometry deviations that were identified as likely contributing factors in the accident. The VTI simulations were conducted using (1) a model representing a nominally maintained loaded flat car; (2) measured track geometry data; (3) measured wheel and rail profiles; (4) a coefficient of friction representative of dry track conditions (the weather was 91° F and dry); and (5) a constant speed of 17 mph. Inter-car forces were not included in the simulations. The resulting forces were compared to established safety criteria to assess the risk of wheel-unloading (i.e. wheel-lift), wheel-climb, or rail-rollover – three common derailment modes that were being considered during the initial phases of the derailment investigation. Although a wide-gage rail-rollover derailment did not occur, the forces were examined to determine if

the potential (onset) for rail rotation about the field-side edge of the rail base existed (and consequently risk of dynamic gage widening), i.e. if the forces were indicative of a risk for the onset of rail-roll over.

Two FRA geometry car surveys taken approximately one month prior to derailment (one on June 4, 2013 and one on June 19, 2013) indicated the existence of a combination track geometry deviation at the POD – namely, a minimally compliant gage deviation (57.81 inches) and a relatively large amplitude short wavelength profile geometry deviation (dip) on both rails (approximately 2 inch amplitude in 40 feet). Figure 3 shows a plot of the measured gage and profile at the derailment site as recorded by FRA's DOTX220 track geometry measurement car on June 4th. For interpretation purposes, the top surface on low rail in the figure on the left was shaded gold and blue to correspond to the same shaded sections in the track geometry data. While neither deviation was considered an exception to the FRA Track Safety Standards (TSS), the TSS in general address specific track conditions that exist in isolation and there sometimes can be a combination of track conditions (none of which individually amounts to a deviation of the TSS) that require remedial action to provide for safe operations over that track.

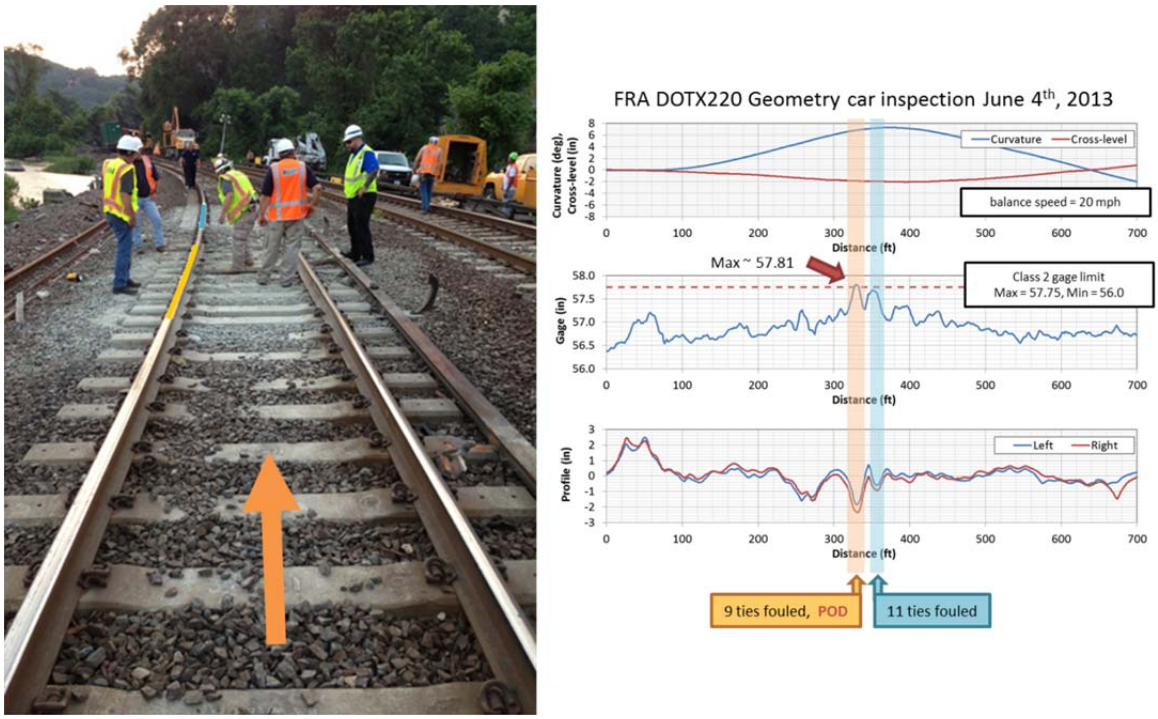

Figure 3: Measured track geometry in derailment zone with low rail (left picture) shaded gold and blue to correspond to the same shaded sections in the track geometry data.

For reference, Figure A1 in appendix A shows all measured track geometry channels used as input to the VTI simulations. The unloaded gage was adjusted to 58.25 inches to reflect the movement of the rails under the fastenings - a condition present at the time of the derailment, described in greater detail later in the Track Condition section below, and not necessarily present at the time of the FRA track geometry surveys. Although wider than the FRA Class 2 gage limit of 57.75 inches, a pre-existing unloaded gage in the range of 58.25 inches is generally not sufficiently wide for wheel drop to occur. An unloaded gage of

this magnitude is an aggravating factor because it reduces the amount of additional dynamic gage widening, from rail movement under vehicle loading, needed for a wide-gage derailment.

As shown in Figure 4, the minimum gage needed to have a wide-gage wheel-drop derailment is a function of the wheel thickness, the wheel back-to-back spacing, and the flange thickness. For a wheel thickness of 5 23/32 inches (the standard dimension of a wide flange wheel), a wheel back-to-back spacing of 53 1/16 inches (the average measured back-to-back), and a flange thickness of 1 ¼ inches (the average measured flange thickness), a gage of approximately 60 inches is needed for wheel drop. As wheels wear to a thinner flange, wheel-drop can also occur with smaller gage.

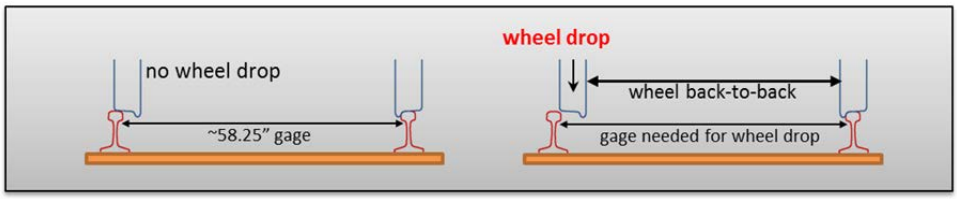

Figure 4: Amount of gage needed for wide-gage wheel-drop derailment is a function of wheel thickness, wheel back-to-back spacing, and flange thickness.

Tables B1 through B2 and Figures B1 through B6 in appendix B summarize the wheel profile measurements taken post derailment. Profile measurements were taken on two sample axles to provide unworn reference profiles (one with new AAR1B wide flange wheels and one with newly trued AAR1B narrow flange wheels) and on three cars (cars 10, 11 and 12) to provide a means of comparing the wheel-rail contact geometry from the derailed car (car 11) to its adjacent cars that did not derail (cars 10 and 12). A comparison of the worn flange thickness is presented in Figures B1 through B6 (all worn flanges were determined to be compliant). Although a mix of narrow flange and wide flange profiles existed on the three cars, the "effective" flange thickness on the high-rail lead axle wheel on each truck was roughly 1 ¼ inches due to the varying amount of wear (see cross-hairs in the upper right plot of Figures B1 through B6). Specifically, the moderate flange wear observed on the wide-flange wheels resulted in flange clearances equivalent to that seen with new narrow-flange wheels. Consequently, the flange thickness on the derailed axle was approximately the same as the other axles that did not derail and thus, from a wheel-rail contact geometry standpoint, it was similarly prone to experiencing a wide-gage wheel-drop derailment. Simulations included both the measured wheel profiles on car 11 and the measured rail profiles taken at the scene, shown in Figure B7.

Table 1 summarizes the VTI Safety Criteria (49 CFR 213.333) published in the FRA VTI Safety Standards that became effective July 11, 2013 to promote VTI safety under various conditions at speeds up to 220 mph. Although applied to higher speed Track Classes, the criteria on wheel forces are also applicable to lower speed Track Classes. The criteria on single wheel vertical load ratio (V_{min}), ratio of lateral-to-vertical wheel load (L/V), and ratio of lateral-to-vertical wheel loads on a truck side (Truck side L/V) were used to assess the likelihood of wheel-unloading, wheel-climb, and rail rollover respectively when examining the vehicle's response to the measured track geometry deviations in the derailment zone.

	Safety Concern	Parameter	Safety Limit		Filter/Window
			Passenger Cars	Other Equipment	
Accelerations	Ride Safety/Ride Quality	Carbody Lateral Acceleration (Transient)	≤0.65g P-P[1]	≤0.75g P-P[1]	1 sec window
		Carbody Lateral Acceleration (Sustained Oscillatory)	≤0.10g RMS_t[2]	≤0.12g RMS_t[2]	4 sec window 4 sec sustained
		Carbody Vertical Acceleration (Transient)	≤1.0g P-P[1]	≤1.25g P-P[1]	1 sec window
		Carbody Vertical Acceleration (Sustained Oscillatory)	≤0.25g RMS_t[2]		4 sec window 4 sec sustained
	Stability/Hunting	Truck Lateral Acceleration (Sustained Oscillatory)	≤0.30g RMS_t[2]		2 sec window 2 sec sustained
Wheel Forces	Wheel Unloading	Single Wheel Vertical Load Ratio	≥0.15		5 foot window
	Wheel-climb Derailment	Single Wheel L/V	$\leq \frac{\tan(\delta)-0.5}{1+0.5\tan(\delta)}$[3]		5 foot window
	Track Shift	Net Axle L/V	$\leq 0.4+\frac{5.0}{Va}$[4]		5 foot window
	Rail Rollover	Truck-side L/V	≤0.60		5 foot window

[1] Peak-to-peak value
[2] Root mean squared with linear trend removed
[3] δ – Flange angle in radians
[4] Va – Vertical axle load in kips

Table 1: Summary of VTI Safety Criteria in 49 CFR 213.333.

While the actual weight and center of gravity are not precisely known, a baseline case was assumed defined by a car having an estimated weight of 280 kips and center of gravity of 93 inches (within the AAR interchange limit of 98 inches maximum). Figure 5 shows the predicted wheel-rail forces in the derailment curve for axle 1 of the baseline case. The plots in the left column correspond to wheel-rail forces on the left rail (low-rail) while the plots in the right column correspond to wheel-rail forces on the right rail (high-rail). For comparison purposes, simulations were conducted with and without the measured track geometry deviations present, an overlay of both results is shown in the plots.

All of the predicted wheel-rail forces in the area around the point of derailment are shown to be well within the FRA VTI Safety Criteria for wheel-unloading, wheel-climb, and rail rollover indicating these modes of derailment were unlikely and that it is unlikely that the derailment was solely due to the combination of track geometry deviations as measured before the accident. Furthermore, Figures C1 and C2 in appendix C show the results of additional simulations conducted to examine parametric variations in vehicle weight and center of gravity respectively. These results indicate that these factors are unlikely to have contributed to this particular derailment for the range of values considered.

Although the predicted wheel-rail forces are well within the FRA VTI Safety Criteria, the FRA criteria do not establish a limit on maximum dynamic vertical wheel loads. Dynamic vertical wheel loads may exceed the capacity of the track or its components and result in progressive (rapid) deterioration under repetitive loading arising from multiple wheel passes. The critical magnitude of wheel load depends on the design and in-service condition of the overall track structure and its components. The maximum dynamic vertical load predicted in the derailment zone is approximately 41 kips. It occurs at the POD as indicated by the blue arrow annotation in Figure 5 and represents a 10% increase in vertical force due to the presence of the profile variations. While this force magnitude may not be a concern for well-maintained track conditions, it is significant for the damaged components (damaged concrete crossties in particular) and deteriorated ballast support conditions (center-bound support in particular) that were present in the derailment area; these track conditions are described in greater detail later in the Track Condition section below.

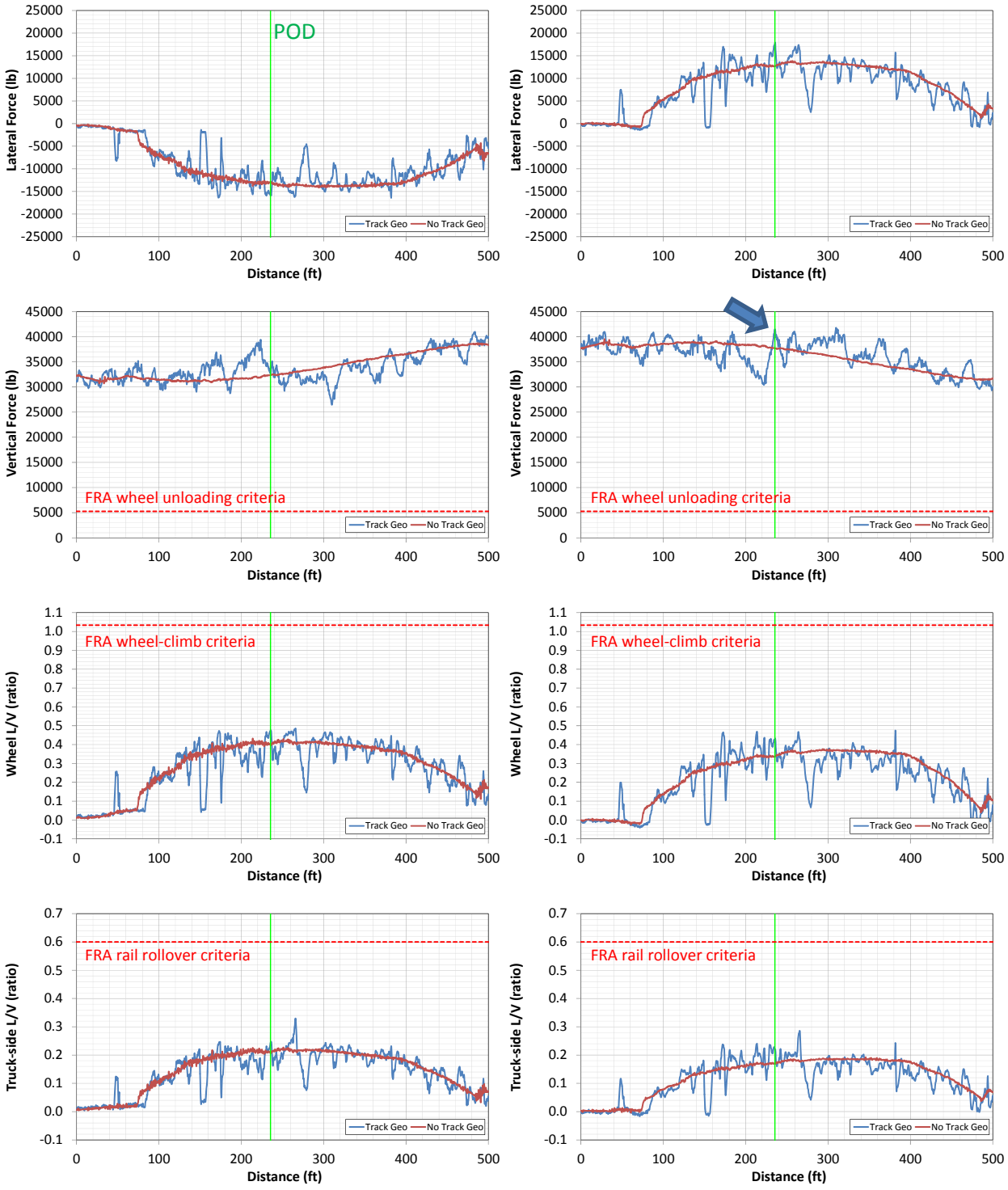

Figure 5: Axle 1 predicted wheel-rail forces in derailment curve for baseline case defined by a car weight of 280 kips and center of gravity of 93 inches: comparison of simulations with and without measured track geometry deviations, plots in the left column are wheel-rail forces on the low-rail, plots in the right column are wheel-rail forces on the high-rail.

Testing[2] and FE modeling[3] were conducted using one new concrete crosstie and five used (damaged[4]) concrete crossties retrieved near the POD to characterize the deflection behavior of the Metro-North crossties[5] under different load and support conditions; these results are described in greater detail later in the Crosstie Characterization section below. Table 2 summarizes the ultimate failure load for each of the load and support conditions analyzed. The ultimate failure load is shown to be highly conditional on the support ballast condition, which is perhaps the most variable quantity among all the track structural parameters. Crosstie damage in the form of cross-section reduction (which is due to dynamic up-and-down pumping action against the ballast and results in reduced flexural capacity) is also shown to have a significant, detrimental effect on the likelihood of sudden, catastrophic tie failure and subsequent wide-gage derailment tendency. For the case of a damaged crosstie supported on a symmetric center-bound support (an idealized case of the derailment conditions) the ultimate failure corresponds to a load of approximately 40 kips as highlighted in blue text. Conversely, the ultimate failure loads for good ballast support conditions are much higher for both crosstie types (new and damaged) and failure appears as cracking under the rail seat.

		Crosstie Condition	
		NEW	Damaged
		peak load (kips)	peak load (kips)
Support Condition	AREMA center negative * (most severe support) 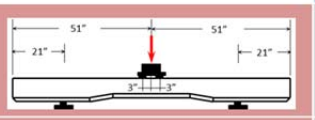	32.3 static load	23.5 static load
	Deteriorated ballast support ** (center-bound support) 	60 dynamic Load	40**** dynamic Load
	Good ballast support ** 	190*** dynamic Load	205*** dynamic Load

* Based on AREMA center negative testing at WJE
** Investigated with FE model
*** Rail seat positive cracking forms rather flexural cracks
**** Derailment conditions

Table 2: Deflection behavior of Metro-North crossties under different load and support conditions, summary of critical loads to reach ultimate failure.

[2] All six crossties were tested to failure tested to failure using the AREMA center negative moment test condition by WJE for the NTSB. The AREMA center negative moment test bends a crosstie in a similar manner to the center-bound ballast support condition, but is a more severe support condition resulting in a lower failure load.
[3] Finite Element (FE) modeling was conducted of the six crossties to estimate their behavior under a representative center-bound ballast support condition.
[4] All five of the damaged concrete crossties retrieved from the fouled ballast zone exhibited a pattern of multiple, evenly spaced, center-bound cracks and abrading on the bottom due to dynamic pumping against the ballast resulting in a reduced height cross-section (i.e. reduced bending resistance).
[5] All six crossties were manufactured circa 1994 in compliance with the Metro-North procurement specification.

The crosstie characterization results in Table 2 indicate that a dynamic vertical load of 41 kips, predicted in the derailment zone in Figure 5, would be sufficient to bend (flex) the previously-damaged-center-bound-supported crossties found near the POD, resulting in further crosstie damage (both further development of center cracks and further reduction in cross-section height due to abrasion of the crosstie bottom) and the rail canting outward as shown in Figure 6. As the rail cants outward, the loaded gage is opened up at the gage corner of the rail head. Figures D1 and D2 in appendix D respectively show the amount of rail cant and loaded gage for a given rail seat deflection of a single crosstie. Since a rail is also restrained against canting by the torsional resistance provided by the rail section and its neighboring crossties, the actual amount of rail cant (and corresponding loaded gage) is likely to be less than that shown in Figures D1 and D2 depending on the condition of a number of crossties in the vicinity of the point of interest, i.e. not just the condition of one crosstie.

The mechanism of gage widening is usually gradual and relatively slow depending on the overall track condition. Crosstie damage and ballast deterioration is likely to have increased (rapidly) with accumulated tonnage and time in the fouled ballast zone found at the derailment site, eventually to the point that 41 kips became sufficient to result in catastrophic failure of the most-severely-damaged-center-bound-supported concrete crossties, Table 2. As described in greater detail later in the Track Condition section below, three crossties retrieved from the track at the POD were found to have failed catastrophically (two of them possibly just prior to the derailment) while many other crossties on both sides of the POD were damaged with center cracks and abrasion on the bottom. The combination of 3 catastrophically failed crossties and multiple damaged crossties were likely sufficient to result in a loaded gage of 60 inches and create the previously mentioned wide-gage scenario in which the rails momentarily spread apart just enough for a wheel-drop derailment of the flanging lead axle of car 11, but not enough for a wheel-drop of the centered trail axle of car 11, Figure 6.

For illustration purposes, Figures D3 through D5 provide a comparison of the wheel-rail contact geometry on axles 1 and 3 of cars 10, 11, and 12 respectively when the rails deflect under load. Each plot is made using the measured profiles and the corresponding measured back-to-back dimensions. All axles are shown to have little margin of safety from a wide-gage wheel-drop derailment. Under such circumstances, small variations in inter-car forces are likely to have led to derailment of axle 1 of car 11, especially in light of the multiple broken crossties whose behavior is less predictable and highly dependent on the specific details associated with the supporting ballast condition.

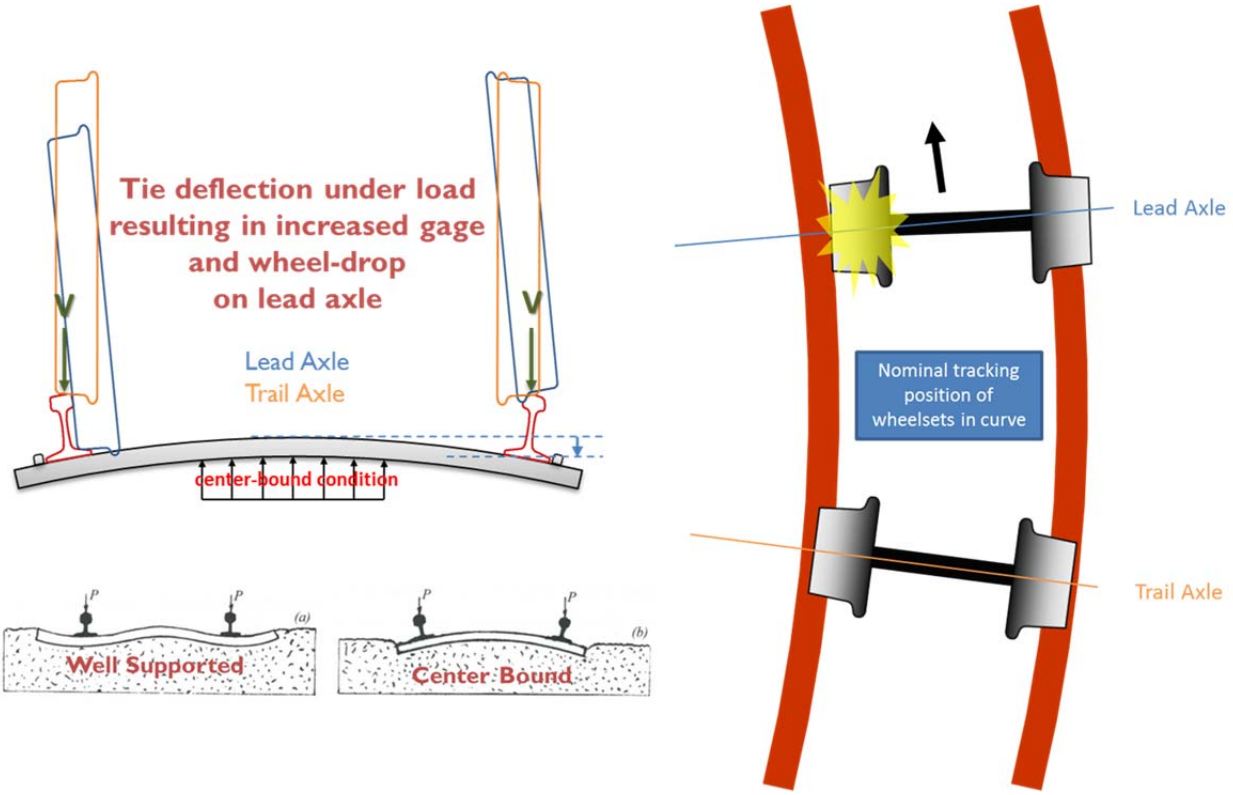

Figure 6: Schematic showing flexing of center-bound supported crosstie deflection under load resulting in increased gage and wheel-drop on the lead axle.

As an indicator of model validation, the motion of the carbody predicted in the simulation was compared to carbody motion that was recorded from a locomotive-mounted camera. Figure 7 shows the carbody roll motion through the derailment zone. Prior to the POD the carbody was leaning slightly towards the low-rail when it suddenly rolls towards the high-rail in a short period of time at the POD in response to the track geometry deviations. A similar carbody motion was observed in the video recorded from a locomotive-mounted camera. This roll motion towards the high-rail near the POD corresponds to the location of maximum dynamic vertical load shown in Figure 5.

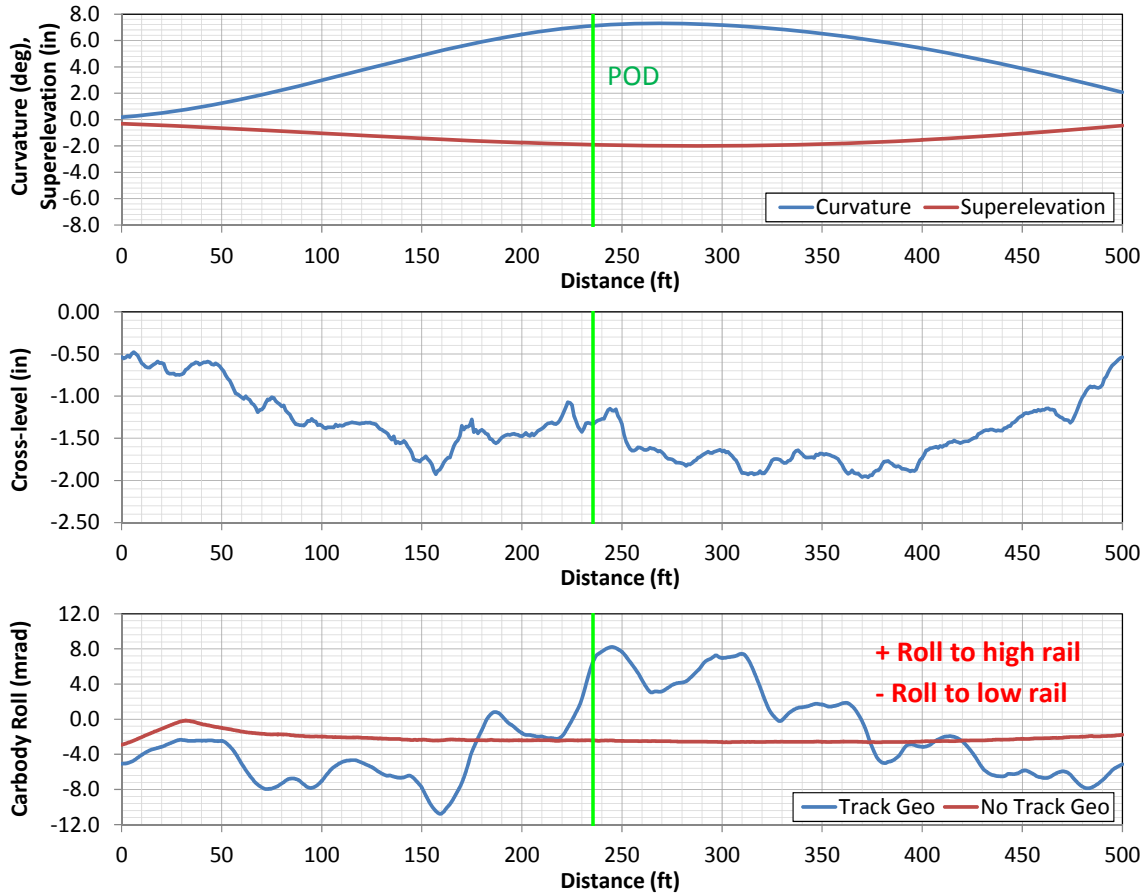

Figure 7: Predicted carbody roll in derailment curve for baseline case defined by a car weight of 280 kips and center of gravity of 93 inches: comparison of simulations with and without measured track geometry deviations.

Wheel-Rail Interaction Summary

The VTI modeling results discussed in the wheel-rail interaction section on the previous pages are intended to offer a better understanding of the derailment circumstances and the manner in which VTI contributes to the deterioration of crossties, ballast, and track geometry. Based on examination of predicted wheel-rail forces, it is unlikely that wheel-unloading, wheel-climb, or rail rollover were the probable derailment mode. Instead, a combination of track related factors produced a loaded gage that resulted in a wide-gage wheel-drop derailment in the curve. Furthermore, because of the tracking position of the truck, it was possible for a wide-gage scenario in which the rails momentarily spread apart just enough for a wheel-drop derailment of the flanging lead axle of car 11, but not enough for a wheel-drop of the centered trail axle of car 11.

The results indicate there is a high risk of wide-gage derailment and sudden, catastrophic crosstie failure when the following conditions exist together:

1. damaged crossties;
2. high dynamic wheel loads; and,
3. poor crosstie support.

While these conditions can occur anywhere, they are more likely to exist together in a fouled ballast track section. In fouled ballast, increased dynamic vertical wheel loads exist due to profile variations, track stiffness variations, or both, Figure 8. The repetitive application of dynamic vertical wheel loads incrementally and permanently damage crossties and ballast. The appearance of pulverized, compacted, or missing ballast that develops gaps at the interface between the ballast and crossties underneath the rail seats eventually evolves into a center-bound crosstie support condition. As crosstie damage develops (i.e. development of center cracks and reduced cross-section), gage is incrementally and permanently widened from its initial position, Figure 9. Hence, gage variations are an indication of the amount of crosstie damage. If the reduction in crosstie cross-section is uneven and larger on the tie ends due to the dynamic up-and-down pumping action of the crosstie-ends, then gaps at the interface between the ballast and crossties underneath the rail seats may further increase, thus worsening the crosstie support condition.

While the presence of fouled ballast and cracks in the surface of a crosstie are a good visual indicator of poor track conditions, track geometry (in particular the combination of gage and profile highlighted above) is a useful objective indicator of a high derailment risk and impending sudden, catastrophic failure of crossties.

1. Profile variations are an indicator of high dynamic wheel loads, damage to crossties, and center-bound support conditions.
2. Gage variations are an indicator of the severity of crosstie damage.

The presence of a large but compliant combination gage and profile deviation (i.e. none of which individually amounts to a deviation of the TSS), indicates a weakened/deteriorated track section that may fail under load, as was the case in the subject derailment.

Further work (not reported here) is ongoing to develop thresholds on combination gage and profile deviations for prioritizing critical fouled ballast track locations.

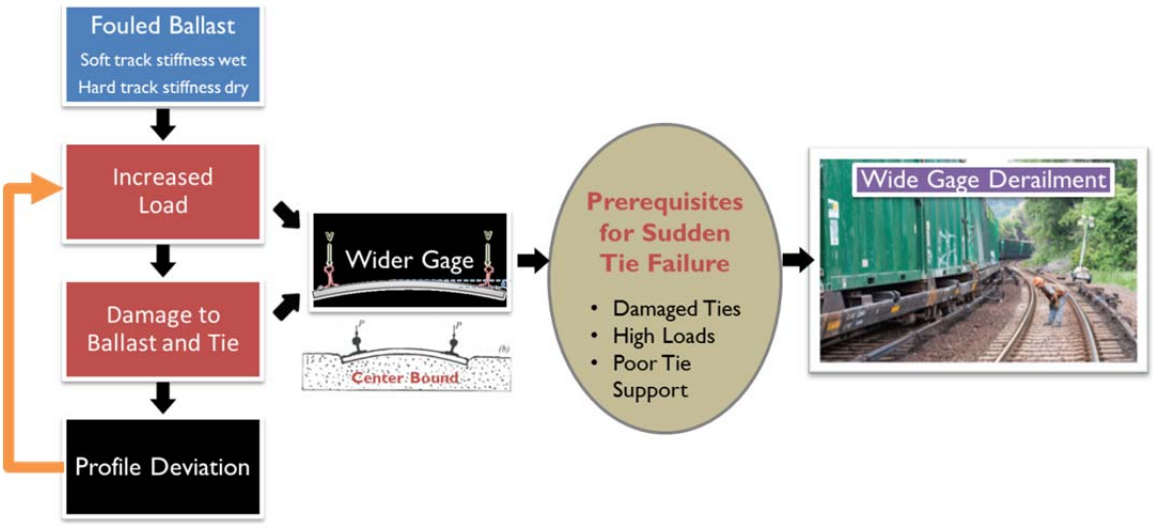

Figure 8: Wide-gage wheel-drop derailment scenario resulting from progressive deterioration and sudden crosstie failure.

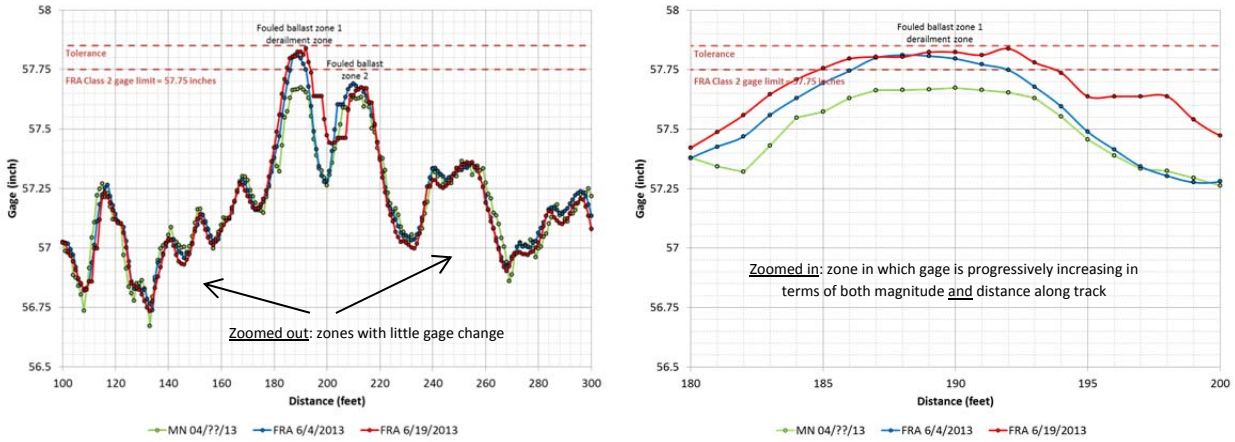

Figure 9: Overlay of track gage in derailment zone recorded on three different dates: zoom out (left) and zoom in (right). Gage in the derailment zone increased significantly in 2 months (green to blue) and then again in 2 weeks (blue to red), an indication that multiple crossties in the derailment zone were deteriorating rapidly.

Note: Figure 14 below is a repeat of Figure 9 above with the size of the plots increased for clarity.

TRACK CONDITION NEAR MILEPOST 9.99

Figure 10 shows multiple views of the derailment site[6] taken shortly after the derailment. Car 11 of the train was traveling northbound through the left-hand curve (first curve of the reverse curve in Figure 10a) at approximately 17 mph when the low-rail-wheel of its lead axle dropped down within the gage between crossties S1 and N1 – crossties were numbered incrementally north and south from POD. The remaining axles of car 11, and cars 12 through 20, derailed in the right-hand curve as a result of further damage to the track. The wide-gage wheel-drop derailment occurred in a fouled ballast zone that encompassed 9 crossties. Four crossties north of the subject fouled ballast zone was another fouled ballast zone that encompassed 11 crossties. Figures 10c, 10d, and 10e show gaps between crossties and ballast, particularly at the crosstie-ends, an indication of significant dynamic (up-and-down) pumping action of the crosstie-ends. Inspections carried out at the derailment site prior to removal of the crossties from the ballast, also revealed that several of the concrete crossties in the fouled ballast zone exhibited a pattern of multiple, evenly spaced, center-bound cracks, Figure 10, and that crosstie S2 was broken, indicative of catastrophic crosstie failure.

Figure 10: Damaged concrete crossties in derailment curve: (10a, upper left) POD looking northbound; (10b, upper right) POD looking southbound; (10c, lower left) POD facing gage side of inside rail; (10d, lower center) POD facing field side of inside rail; and, (10e, lower right) gaps at the crosstie-ends on inside of curve.

[6] The gage rods shown in Figure 10 near the POD were installed post derailment.

While visual inspection of the surface indicated that the fouled ballast appeared dry, inspection carried out after digging out and removing the crossties revealed that water was trapped below the crossties in the fouled ballast, Figure 11.

Figure 11: Presences of water beneath crossties and ballast layer.

Removal of the crossties near the POD, Figure 12, further revealed that crossties N1 and S1 were also broken in the vicinity of the rail seat of the high rail, indicative of catastrophic crosstie failure. In addition, the concrete crossties in this zone were abraded on the bottom due to dynamic up-and-down pumping action against the ballast. The center-bound cracks and the greater abrasion towards the ends of the crossties (to the point of exposing reinforcement strands) are indicators that the crossties were center-bound, in which the center of the crossties is supported while the ends behave like cantilever beams, as a result of the fouled ballast condition, see illustration in Figure 13.

Figure 12: Damaged concrete crossties in derailment curve:
(12a, upper left) POD looking northbound – S2 broken;
(12b, middle left) crossties at POD after removal – N1, S1, and S2 broken;
(12c, lower left) close-up of crossties at POD after removal – reduced section of crossties;
(12d, upper right) characterization of center cracks on crossties near POD;
(12e, middle right) ends of crossties near POD; and,
(12f, bottom right) typical bottom of crossties near POD.

Figure 13: Indicators of center supported crossties (center-bound crossties).

It is likely that the profile deviations developed over time as a result of degradation of the ballast support condition due to ballast fouling (localized change in track stiffness) and many passes of dynamic wheel/rail forces. As a result of the damaged crossties (multiple crossties with center-bound cracks and reduced height cross-section – i.e. reduced bending resistance), the dynamic wheel/rail forces, and the poor support condition (center-bound crosstie), the crossties were flexing under load producing a maximum gage of 57.81 inches (larger than the FRA class 2 limit of 57.75 inches but not considered a defect because of a 0.1 inch tolerance applied to geometry car measurements). While the gage recorded on June 4th is below that which is needed for wheel drop (typically a gage between 59.5 and 60 inches is needed for wheel drop depending on the flange thickness, etc.), the gage was progressively increasing in terms of both magnitude and distance along track with accumulated tonnage and time, Figure 14; an indication that the track conditions, in particular the crossties, were deteriorating relatively fast considering the tonnage present on that line. The gage was incrementally and permanently widened from its initial position by the repetitive application of vertical wheel loads. It is likely that progressive track failure was occurring under a cycle of repeated dynamic loading, Figure 15, that involved individual crossties becoming increasingly damaged (some to the point of sudden catastrophic failure) at the same time that damage on neighboring crossties was developing, and so on.

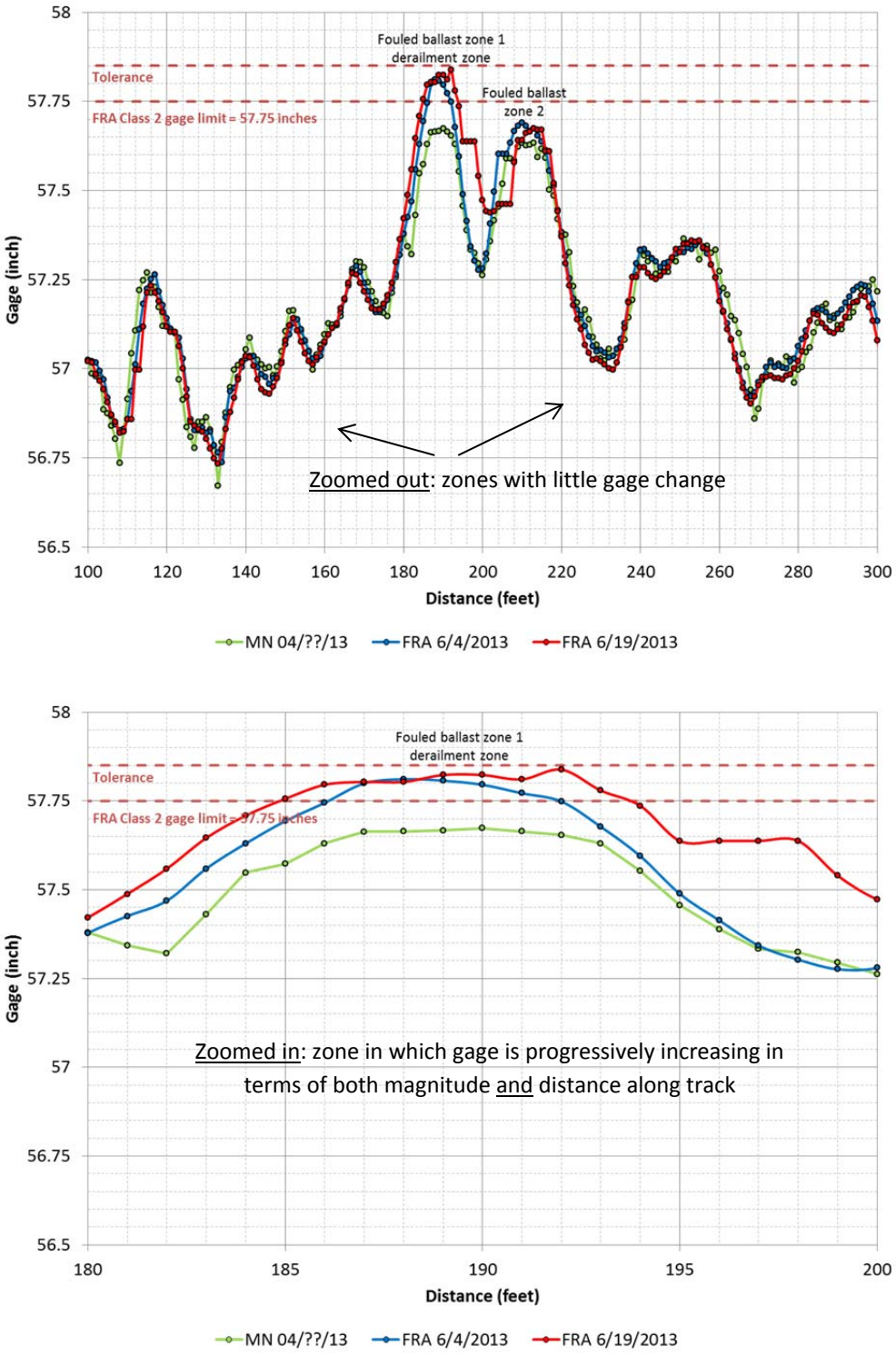

Figure 14: Overlay of track gage in derailment zone recorded on three different dates: zoom out (top) and zoom in (bottom). Gage in the derailment zone increased significantly in 2 months (green to blue) and then again in 2 weeks (blue to red), an indication that multiple crossties in the derailment zone were deteriorating rapidly.

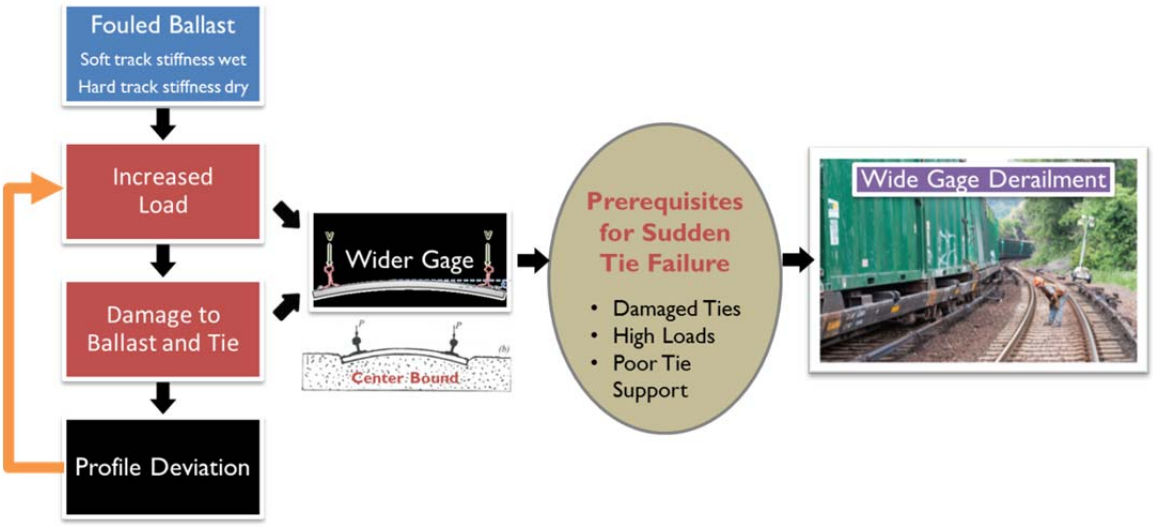

Figure 15: Wide-gage wheel-drop derailment scenario resulting from progressive deterioration and sudden crosstie failure.

During the time of the accident, the New York City area had been experiencing a heat wave. The daytime high temperature had been above 90° F each of the three days preceding the derailment. The weather at the time of the accident was reported as 91° F with clear skies, no precipitation. As a result of the high temperatures, both rails were spread towards their respective field side increasing the unloaded gage to 58.25 inches by slipping under the insulator shoulders, Figure 16.

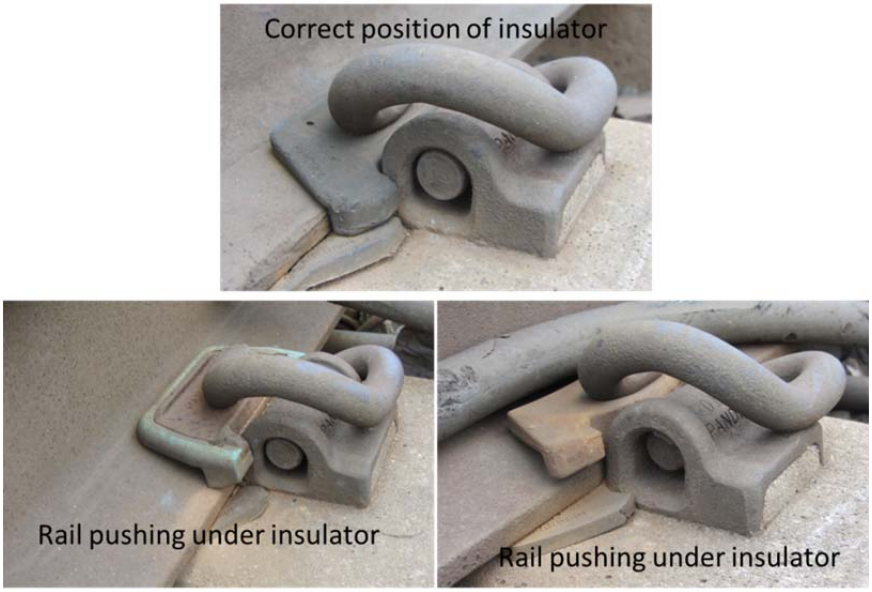

Figure 16: High and Low Rails Pushing Under the Insulator Clips.

CROSSTIE CHARACTERIZATION, DEFLECTION BEHAVIOR OF METRO-NORTH CROSSTIES UNDER DIFFERENT LOAD AND SUPPORT CONDITIONS

Testing[7] was conducted using one new concrete crosstie and five used (damaged) concrete crossties retrieved near the POD to characterize the deflection behavior of the Metro-North crossties[8] under load. The five damaged included crossties leading to the POD (namely, S3, S4, and S5) and crossties located some distance after the POD (namely, N10 and N16) – crossties were numbered incrementally north and south from POD, Figure 17. Because the three crossties nearest the POD were already broken (N1, S1, and S2), testing of those crossties was not possible.

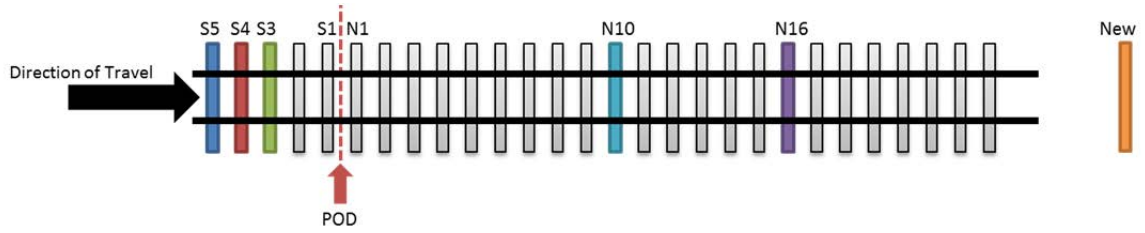

Figure 17: Numbering convention of concrete crossties in derailment curve.

AREMA center negative moment tests[9] were conducted on the selected concrete crossties. In order to evaluate their ultimate center negative moment capacities, loads were increased until the crossties failed catastrophically. Although the crossties were tested upside down with their rail seats resting on two rubber supports, the AREMA tie center negative moment test configuration bends the tie in a similar manner to the center-bound ballast support condition, Figure 18. However, because the AREMA configuration represents a more severe support condition than that found in-service with ballast, it results in a lower load to failure than would be seen when supported by ballast in the field.

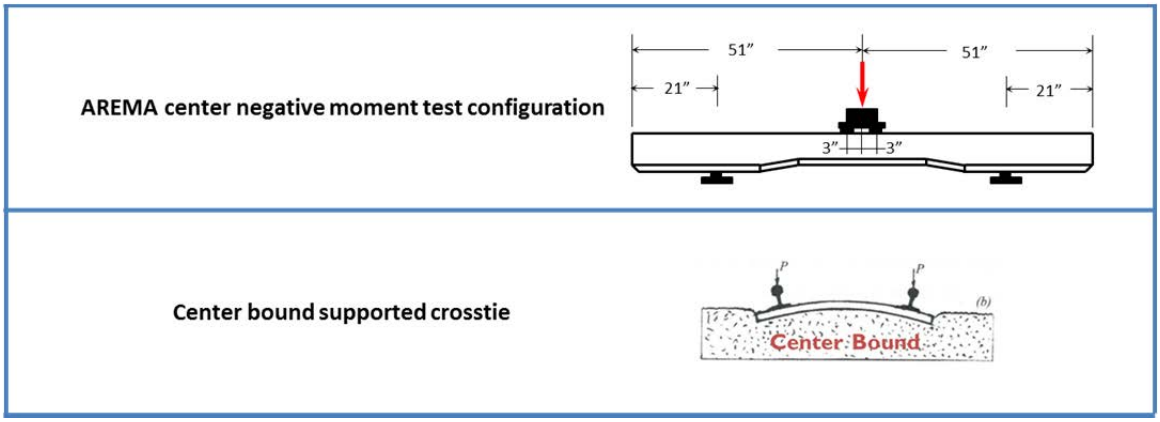

Figure 18: Comparison between AREMA tie center negative moment test configuration and a center-bound supported crosstie.

[7] All six crossties were tested to failure tested to failure using the AREMA center negative moment test condition by WJE for the NTSB.
[8] All six crossties were manufactured circa 1994 in compliance with the Metro-North procurement specification.
[9] Manual for Railway Engineering, Chapter 30, Part 4: Concrete Ties. American Railway Engineering and Maintenance-of-Way Association, 2010.

All five of the concrete crossties retrieved from the fouled ballast zone exhibited damage similar to that shown in Figure 19 – namely, a pattern of multiple, evenly spaced, center-bound cracks and abrading on the bottom due to dynamic up-and-down pumping action against the ballast resulting in a reduced height cross-section (i.e. reduced bending resistance).

Figure 19: Concrete crossties in derailment curve:
(19a, upper left) POD looking northbound – S2 broken;
(19b, middle left) crossties near POD after removal – N1, S1, and S2 broken;
(19c, lower left) close-up of crossties near POD after removal – reduced section of crossties;
(19d, upper right) characterization of center cracks on crossties near POD;
(19e, middle right) ends of crossties near POD; and,
(19f, bottom right) typical bottom of crossties near POD.

Figure 20 shows the measured load-deflection for each of the tested crossties. After the initial linear response around 0.05 inch mid-span deflection, flexural cracks develop. The peak load in each curve at around 0.4 inch mid-span deflection corresponds to sudden, catastrophic failure of the crosstie (i.e. shear failure or ultimate failure of the crosstie). The ultimate failure load is higher for the new crosstie, approximately 32.3 kips, as might be expected. Crossties S3 and S4 (which were the closest to the POD and most representative of crossties N1, S1, and S2 in terms of reduced cross-section) exhibited the lowest ultimate failure loads, crosstie S3 being the lowest – approximately 23.5 kips.

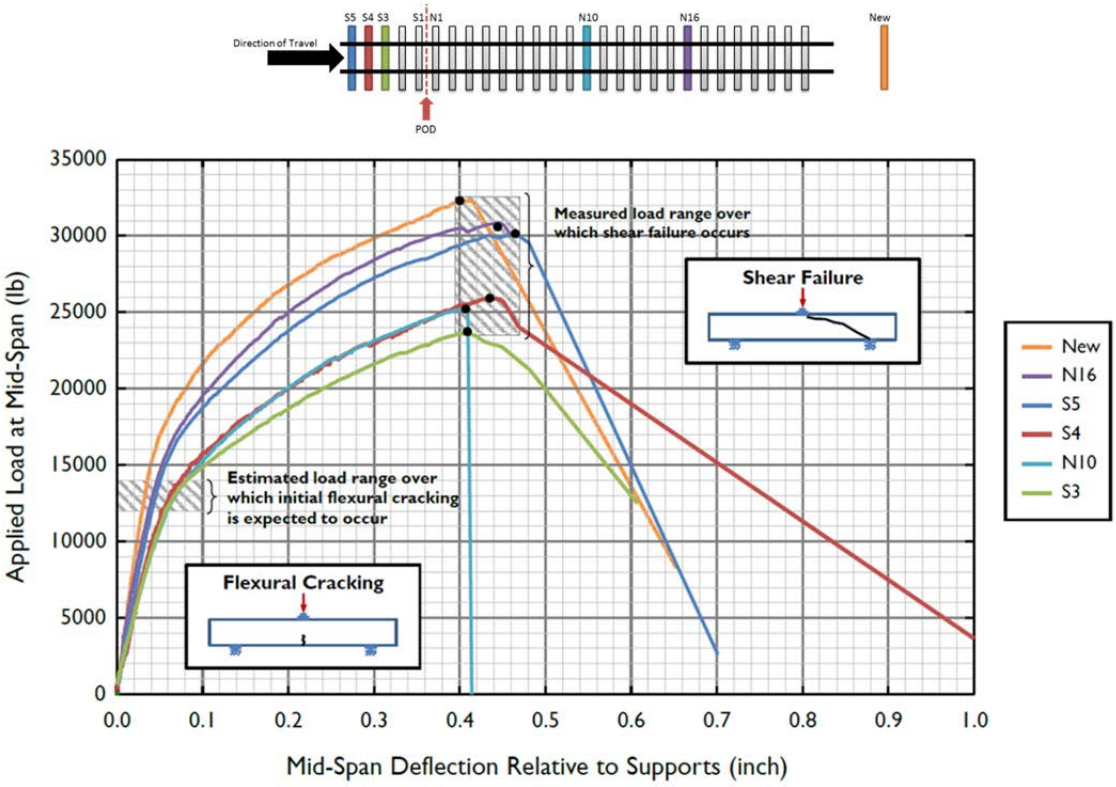

Figure 20: Measured load-deflection behavior of Metro-North concrete crossties using AREMA center negative test configuration.

While testing demonstrated the crossties behavior under the extreme 3-point bending AREMA center negative test configuration, finite element (FE) analyses were conducted using one model representing a new crosstie and one model representing damaged crosstie S3 to predict the behavior of Metro-North concrete crossties under different load and support conditions. In this case, the damaged crosstie model is the same as the new crosstie model with 1 inch of concrete material removed from the tie bottom across the entire tie length – the exact geometry of the damaged crosstie was not used. Figure 21 shows the load-deflection behavior for 3 support conditions – namely, (1) an AREMA center negative supported crosstie, (2) a symmetric center-bound supported crosstie, and (3) a well-supported crosstie. Deflection on the horizontal axes is express as "deflection under rail seat" which is indicated by the blue arrow in the schematic in Figure 21(a). This is equivalent to the "mid-span deflection used in Figure 20. In Figures 21(a) and 21(b), the AREMA static simulations are compared to test results as an indicator of model validity. While the goal was to load the crossties to complete failure in the analyses, because the

ultimate failure of concrete crossties is often sudden and catastrophic, it is very difficult for a static simulation to capture the behavior near around the peak. The simulation curves agree reasonably well with the test curves, though they stop at lower deflections and slightly lower peak loads than the test curves. Simplified modeling of the concrete-reinforcement interface may explain the discrepancies.

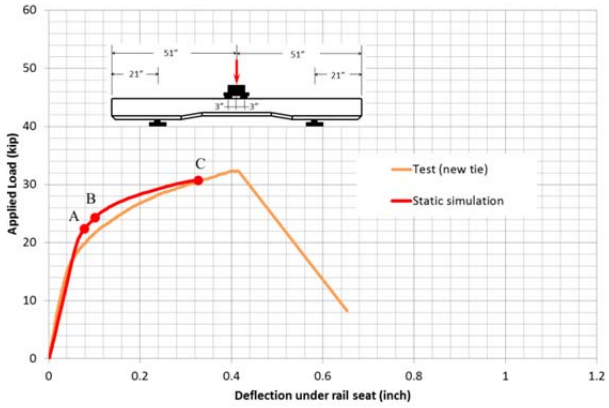

(a) NEW crosstie, AREMA negative center support

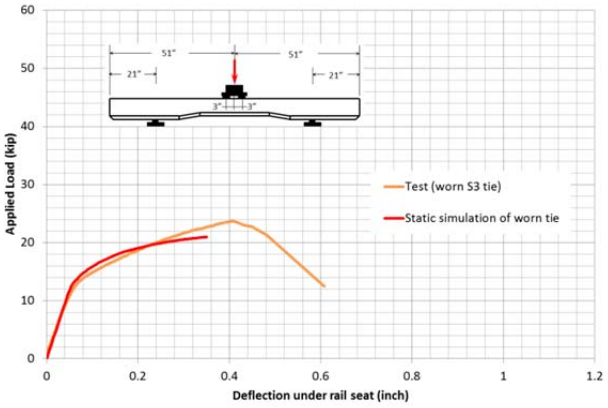

(b) damaged crosstie S3, AREMA negative center support

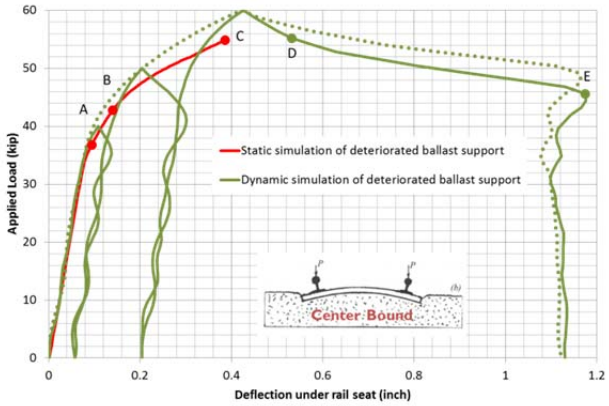

(c) NEW crosstie, center-bound support

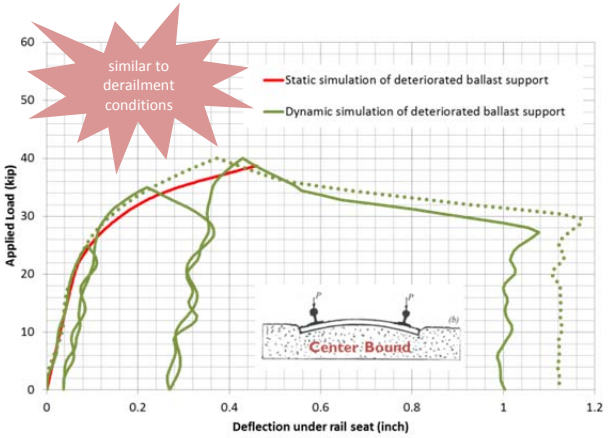

(d) damaged crosstie S3, center-bound support

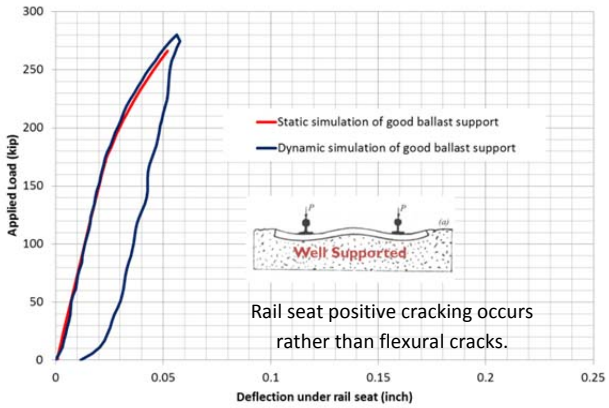

(e) NEW crosstie, good ballast support

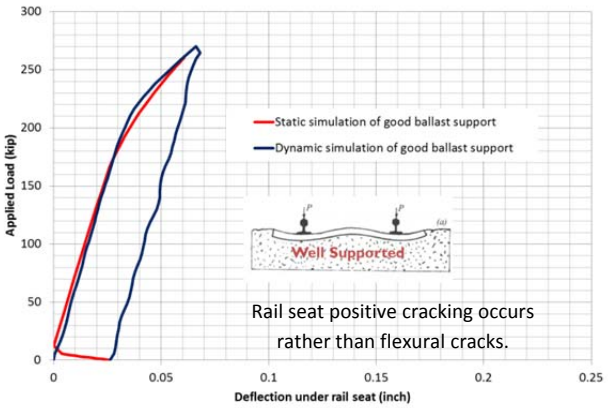

(f) damaged crosstie S3, good ballast support

Figure 21: Measured and predicted load-deflection behavior of Metro-North concrete crossties under different load and support conditions.

For the purposes of this study, the ultimate failure loads predicted here are considered to be equivalent wheel loads by assuming the crosstie directly under the wheel was analyzed and it supports 50% of the total wheel load. The percentage of wheel load seen by the crosstie directly under the wheel is strongly dependent on the condition of the ballast support – tracks with higher track stiffness tend to concentrate wheel loads locally to a fewer number of crossties increasing the percentage while tracks with softer track stiffness tend to distribute wheel loads amongst more crossties decreasing the percentage. In light of the fouled ballast conditions noted at the derailment site, a percentage (50%) was assumed.

Figure 22 shows the model of deteriorated ballast support used in the analyses shown in Figures 21(c) and 21(d) above for representing the center-bound support condition found at derailment location. The gap at the interface between the ballast and crossties near the crosstie ends, Δh, are intended to represent the combination of missing/pulverized ballast and uneven wear on the crosstie bottom near the crosstie ends. A gap of 2 inches was used to represent these combined conditions.

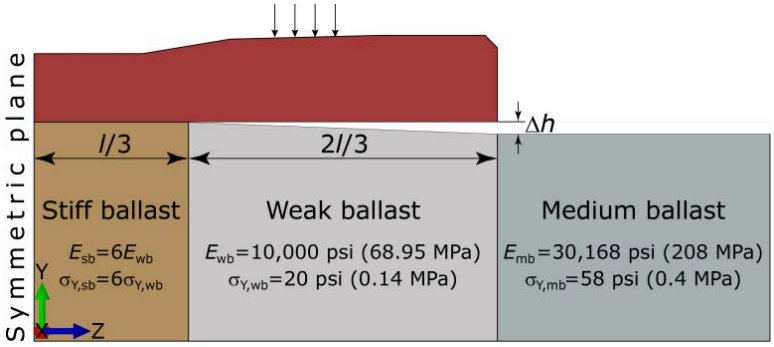

Figure 22: Model of deteriorated ballast support representing center-bound support condition found at derailment location, cases Figure 21(c) and 21(d).

While the loads in the AREMA center negative support condition cases are applied statically, the cases involving the center-bound support conditions were conducted using both a statically applied load and a dynamically applied load to better represent the type of loading that may be experienced in the field. Figure 23 shows the time history of dynamic load applied the analysis above with the new crosstie and center-bound support condition, case Figure 21(c). A similar, but lower magnitude time history is applied in the analysis above with the damaged crosstie S3 and center-bound support condition, case Figure 21(d).

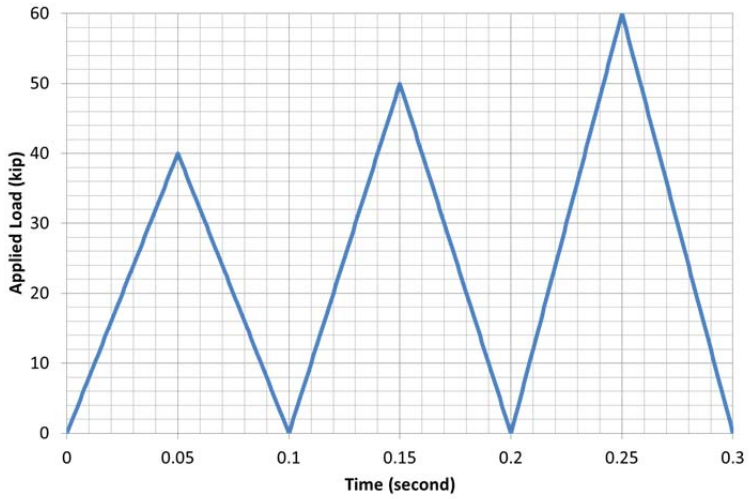

Figure 23: Time history of dynamic load applied the case with the new crosstie and center-bound support condition, case Figure 21(c).

Figure 24 shows three stages of cracking in the static load analysis above with the new crosstie and the AREMA center negative test support condition, case Figure 21(a).

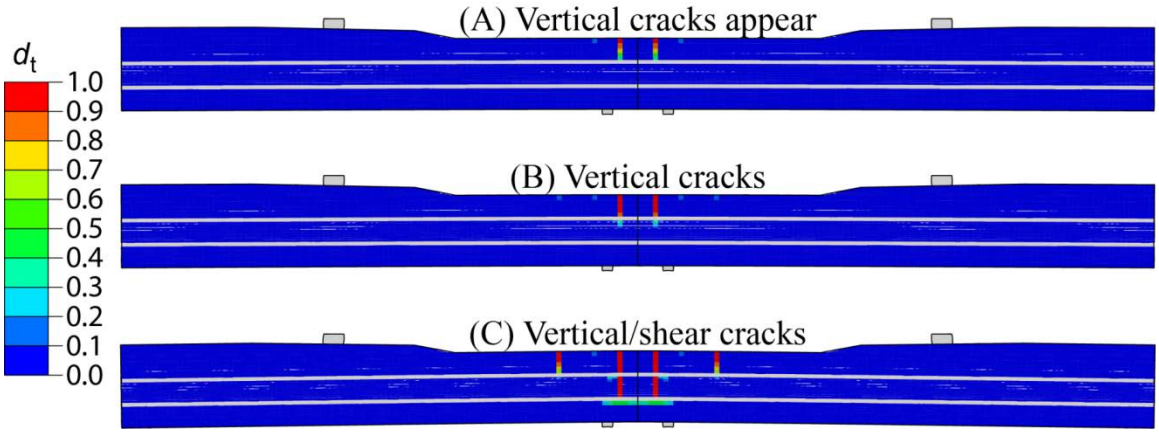

Figure 24: Three stages of cracking in the static load analysis with the new crosstie and the AREMA center negative test support condition, case Figure 21(a).

Figure 25 shows three stages of cracking in the static load analysis above with the new crosstie and the center-bound support condition, case Figure 21(c).

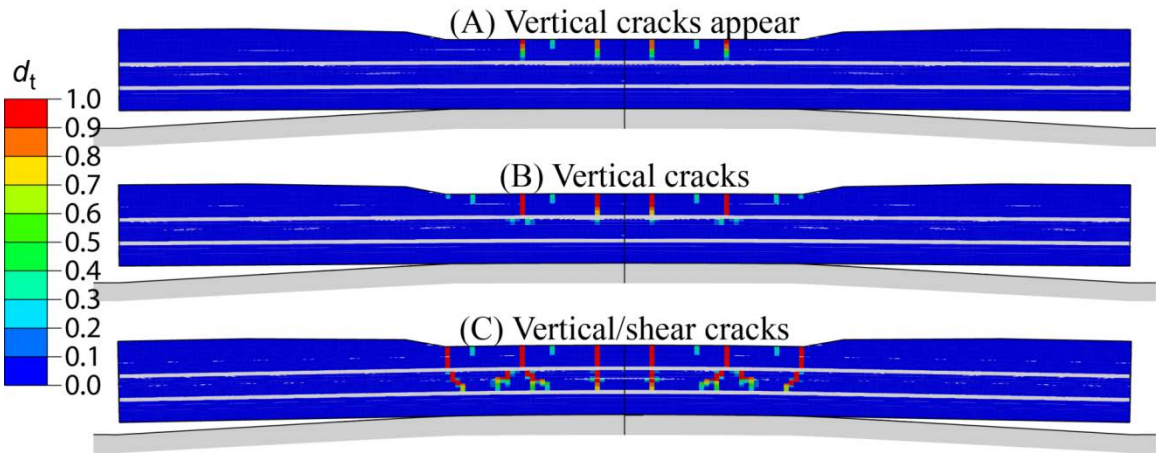

Figure 25: Three stages of cracking in the static load analysis with the new crosstie and the simulated center-bound support condition, case Figure 21(c).

Figure 26 shows three stages of sudden catastrophic failure in the dynamic load analysis with the new crosstie and the simulated center-bound support, case Figure 21(c).

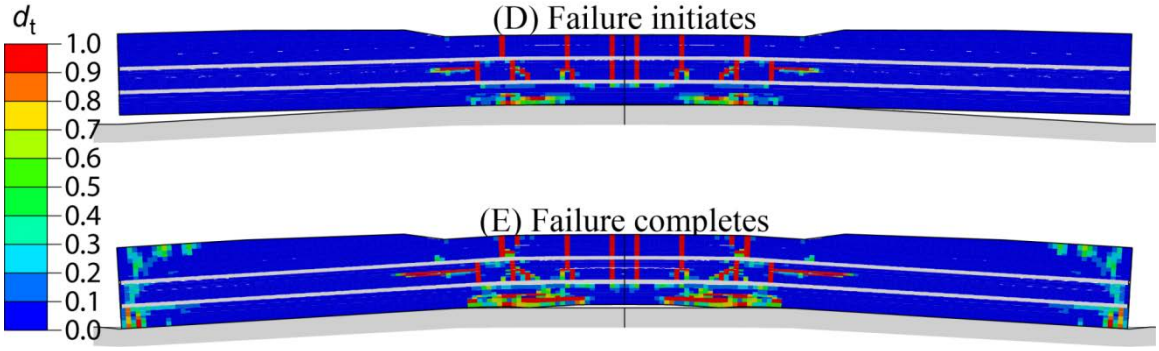

Figure 26: Stages of sudden catastrophic failure in the dynamic load analysis with the new crosstie and the simulated center-bound support, case Figure 21(c).

The FE analyses described above investigated the effects of loading and support conditions on ultimate tie failure. The results are meant to provide an estimate of failure loads under different conditions. Further on going work is being conducted to examine the effect of other ballast and loading assumptions on ultimate crosstie failure load. For example, Figure 27 shows results for the damaged crosstie S3 and the simulated center-bound support, same as case Figure 21(b), including cyclic 35 kip dynamic load case. Under these circumstances ultimate crosstie failure may happen at a lower load.

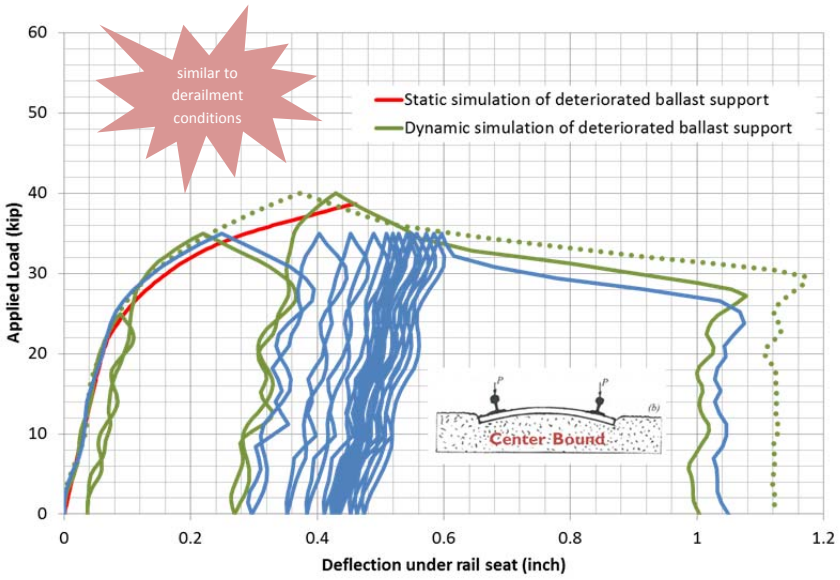

Figure 27: Load-deflection behavior for the damaged crosstie S3 and the simulated center-bound support, same as case Figure 21(b), including cyclic 35 kip dynamic load case.

ACKNOWLEDGEMENT

The work described in the paper was sponsored by the Office of Research and Development, Federal Railroad Administration, U.S. Department of Transportation.

APPENDIX A – TRACK GEOMETRY INPUTS TO SIMULATION

Figure A1 shows the measured track geometry used as input to the VTI simulations having the unloaded gage adjusted to 58.25 inches to reflect the movement of the rails under the insulator clips - a condition present at the time of the derailment (described in greater detail in the Track Condition section) and not necessarily at the time of the FRA track geometry surveys.

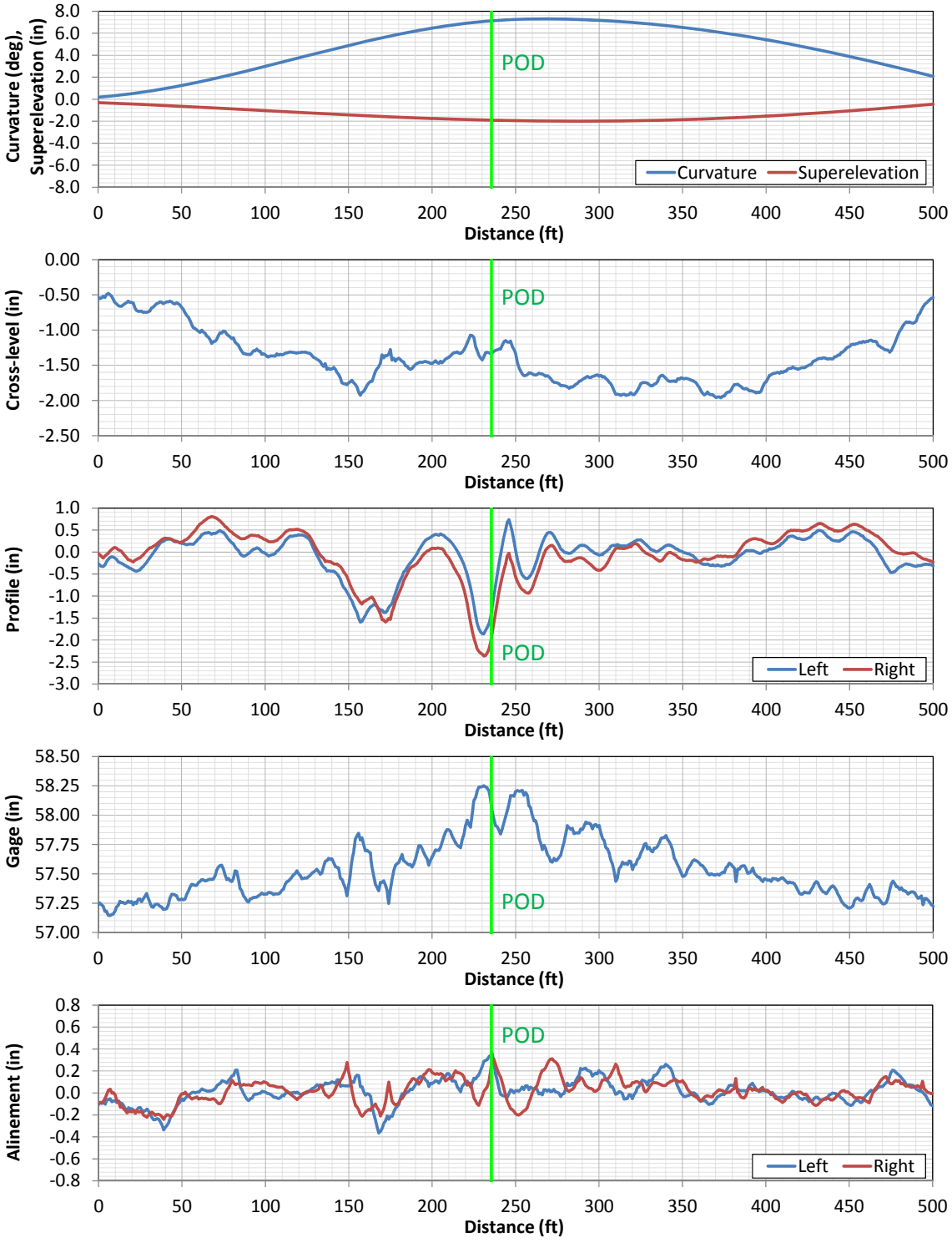

Figure A1: Measured track geometry data used in simulation: curvature, superelevation, crosslevel, profile, gage, and alinement.

APPENDIX B – WHEEL AND RAIL PROFILE MEASUREMENTS

Tables B1 though B2 and Figures B1 through B6 summarize the wheel profile measurements taken post derailment. Profile measurements were taken on sample axles (one with new AAR1B wide flange wheels and one with newly trued AAR1B narrow flange wheels) to provide a reference for the various AAR1B wide flange and narrow flange profiles observed on the cars and on three cars (cars 10, 11 and 12) to provide a means of comparing the wheel-rail contact geometry from the derailed car (car 11) to its adjacent cars that did not derail (cars 10 and 12).

sample	new axle	L	out of car	AAR1B wf, new	
		R	out of car	AAR1B wf, new	
	trued axle	L	out of car	AAR1B nf, newly trued	
		R	out of car	AAR1B nf, newly trued	
Car 10 40113	Axle 1	1L	in car	AAR1B wf	
		1R	in car	AAR1B wf	
	Axle 2	2L	in car	AAR1B wf	
		2R	in car	AAR1B wf	
	Axle 3	3L	in car	AAR1B wf	
		3R	in car	AAR1B wf	
	Axle 4	4L	in car	AAR1B wf	
		4R	in car	AAR1B wf	
Car 11 638345	Axle 1	1L	in car	AAR1B wf	} Derailed axle
		1R	in car	AAR1B wf	
	Axle 2	2L	in car	AAR1B wf	
		2R	in car	AAR1B wf	
	Axle 3	3L	out of car	AAR1B nf, recently trued	
		3R	out of car	AAR1B nf, recently trued	
	Axle 4	4L	in car	AAR1B nf, recently trued	
		4R	in car	AAR1B nf, recently trued	
Car 12 638391	Axle 1	1L	in car	AAR1B nf, worn	
		1R	in car	AAR1B nf, worn	
	Axle 2	2L	out of car	AAR1B wf	
		2R	out of car	AAR1B wf	
	Axle 3	3L	out of car	AAR1B wf	
		3R	out of car	AAR1B wf	
	Axle 4	4L	in car	AAR1B wf	
		4R	in car	AAR1B wf	

Table B1: Summary of measured wheel profiles.

Car initial&#	Axle 1	Axle 2	Axle 3	Axle 4
USWX 638391 (Car 12)	53 1/8	53 1/8	53 1/16	53 1/8
USWX 638345 (Car 11)	53 1/16	53 1/16	53 1/16	53 1/16
USWX 40113 (Car 10)	53	53 1/8	53 1/8	53

Table B2: Summary wheel back-to-back spacing of axles on which wheel profiles were measured.

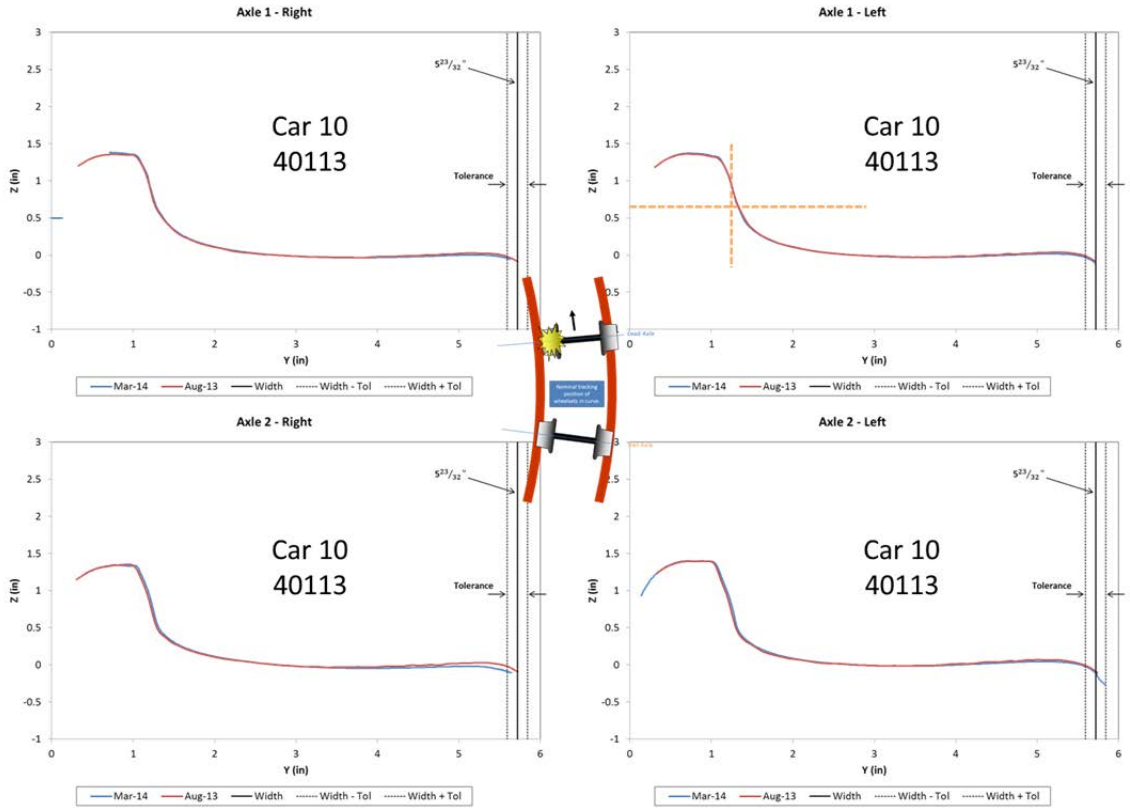

Figure B1: Wheel profiles on car 10, lead truck; left and right are when looking from the front of the car backwards.

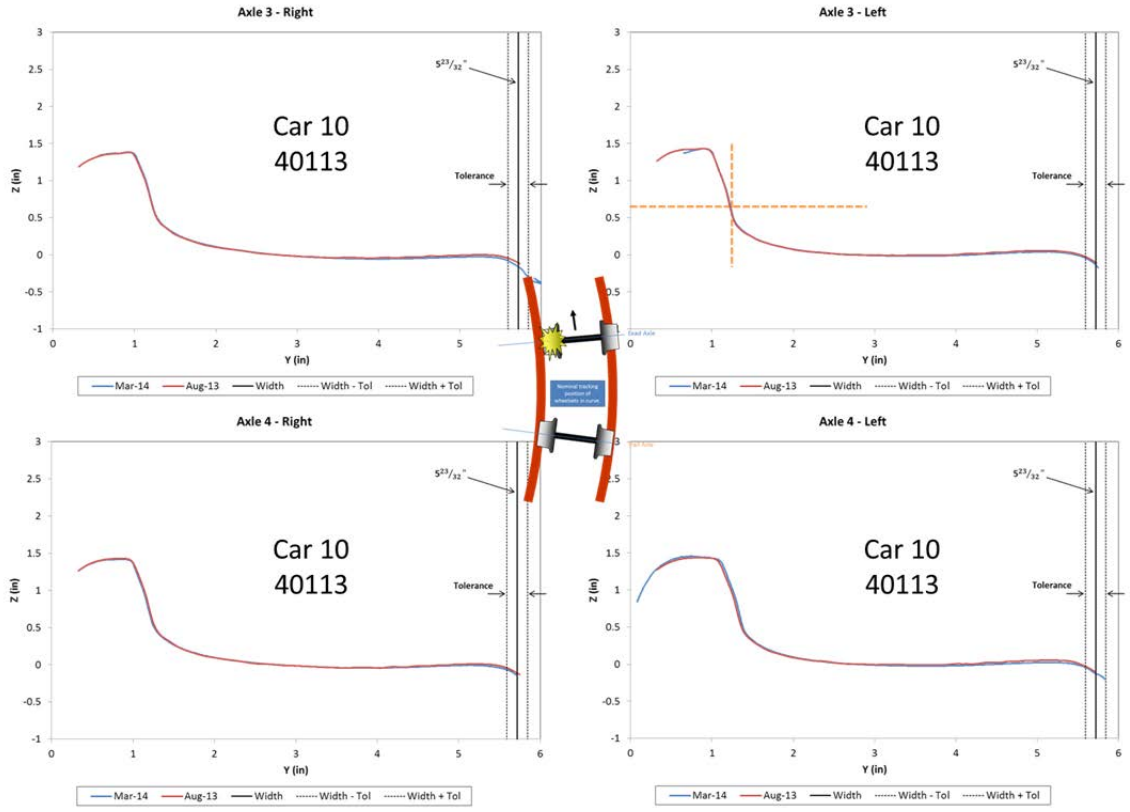

Figure B2: Wheel profiles on car 10, trail truck; left and right are when looking from the front of the car backwards.

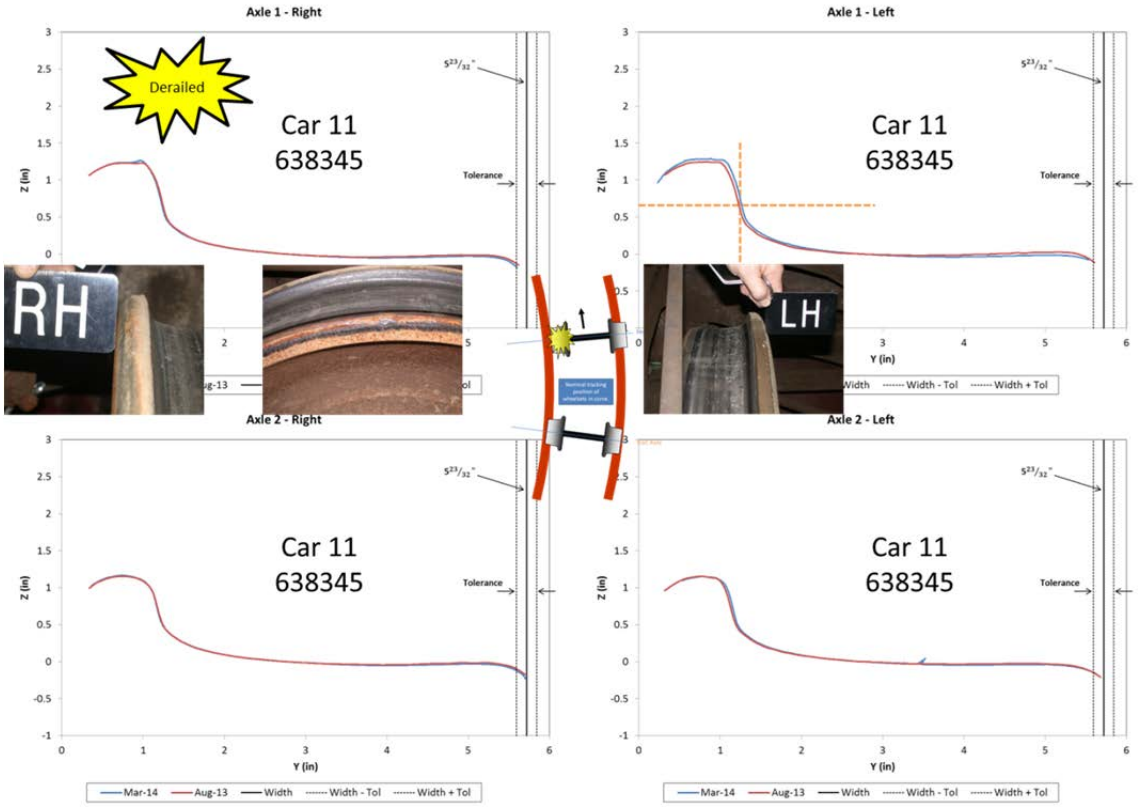

Figure B3: Wheel profiles on car 11, lead truck; left and right are when looking from the front of the car backwards.

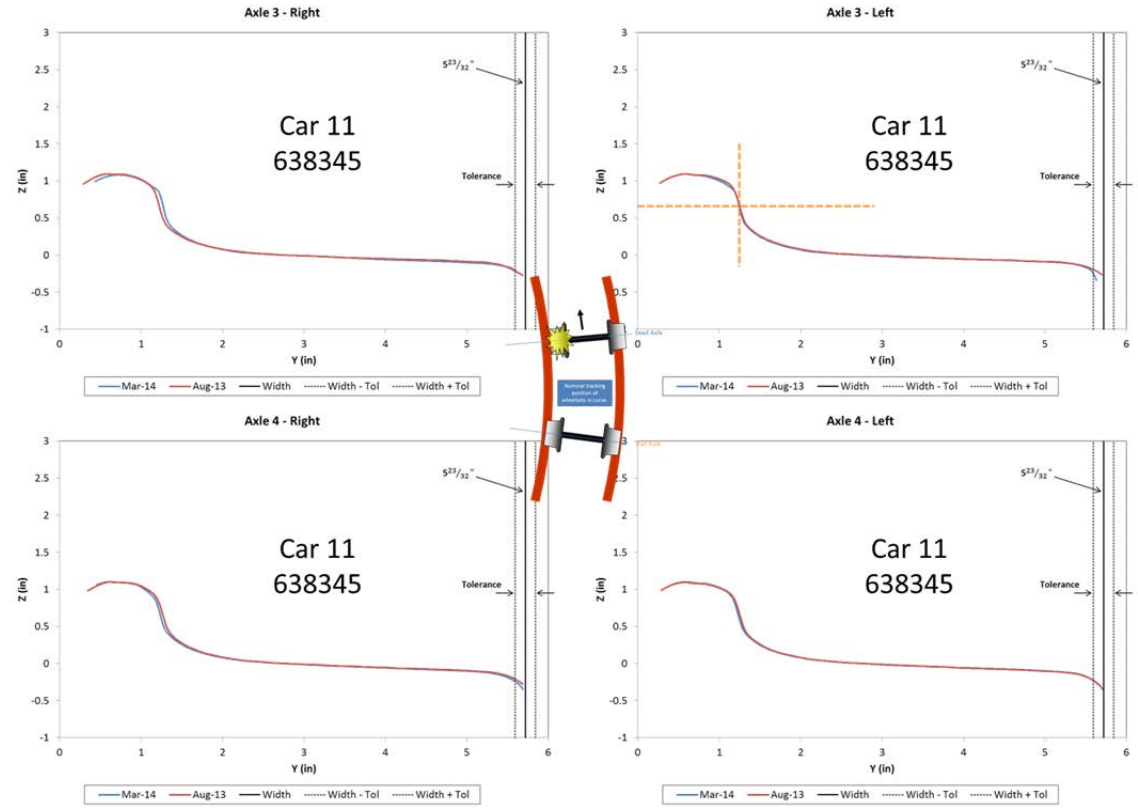

Figure B4: Wheel profiles on car 11, trail truck; left and right are when looking from the front of the car backwards.

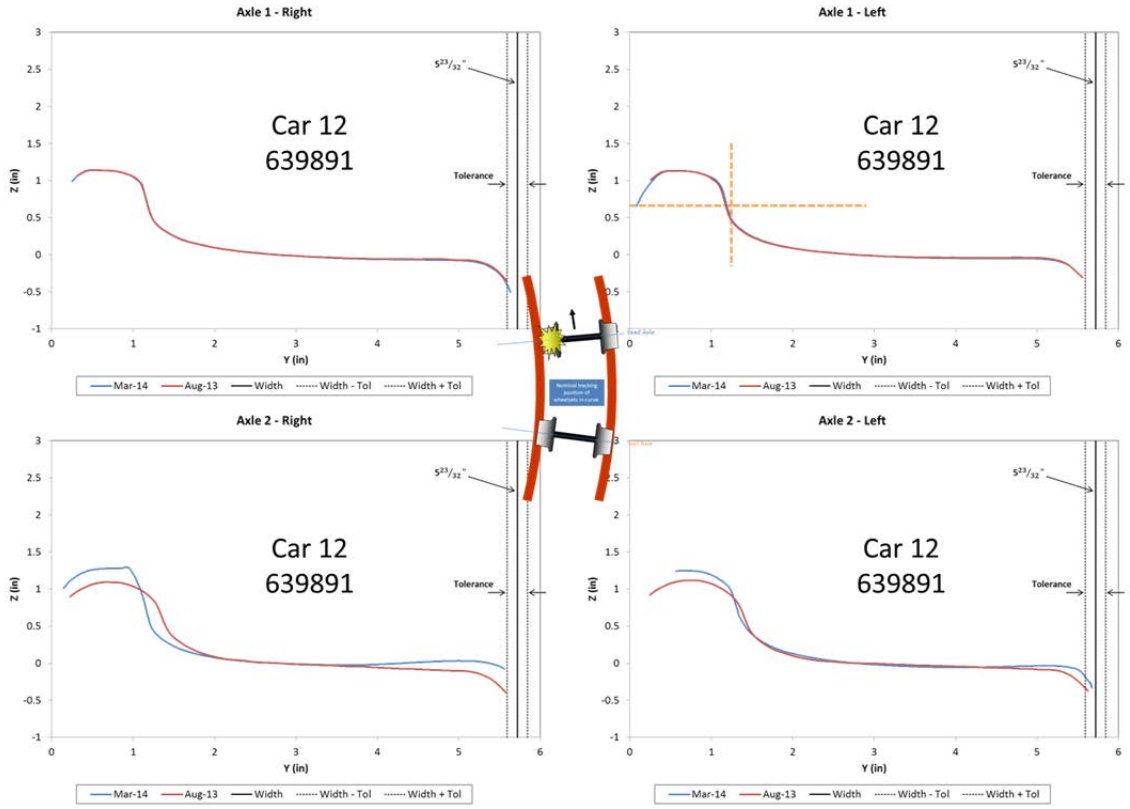

Figure B5: Wheel profiles on car 12, lead truck; left and right are when looking from the front of the car backwards.

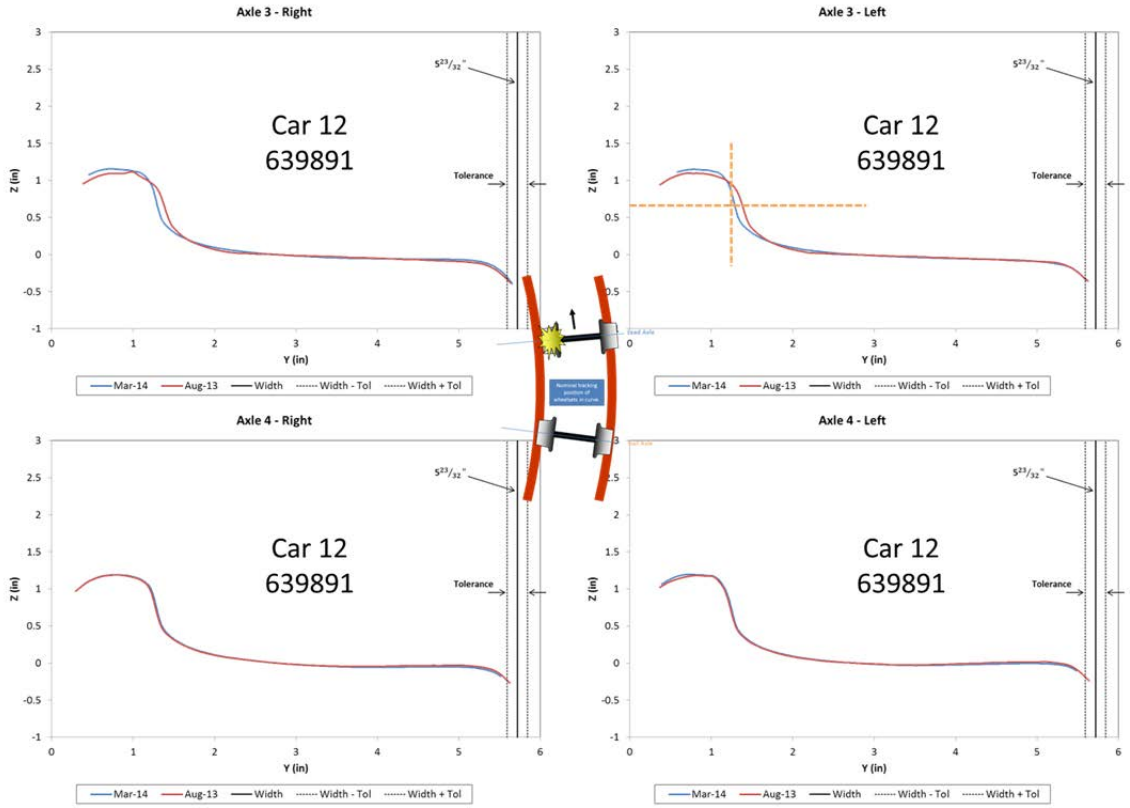

Figure B6: Wheel profiles on car 12, trail truck; left and right are when looking from the front of the car backwards.

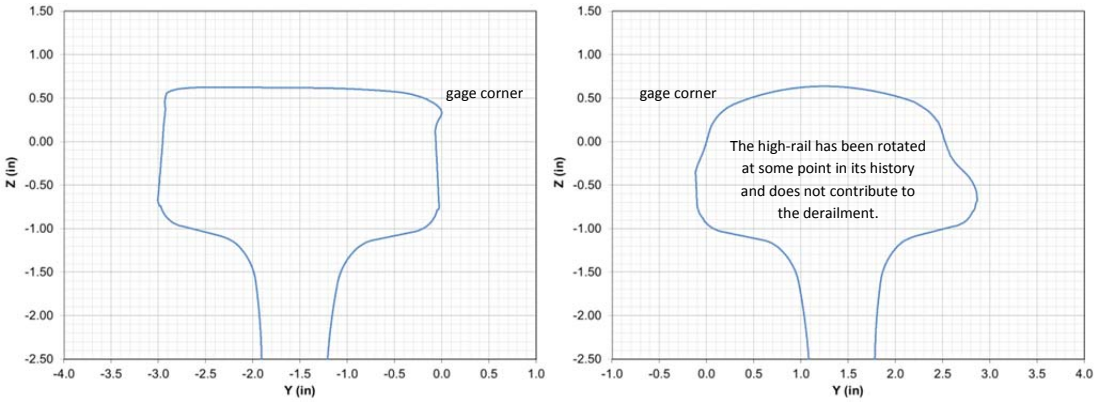

Figure B7: Rail profiles taken near POD (low-rail left, high-rail right).

APPENDIX C – THE EFFECTS OF CENTER OF GRAVITY AND CAR WEIGHT

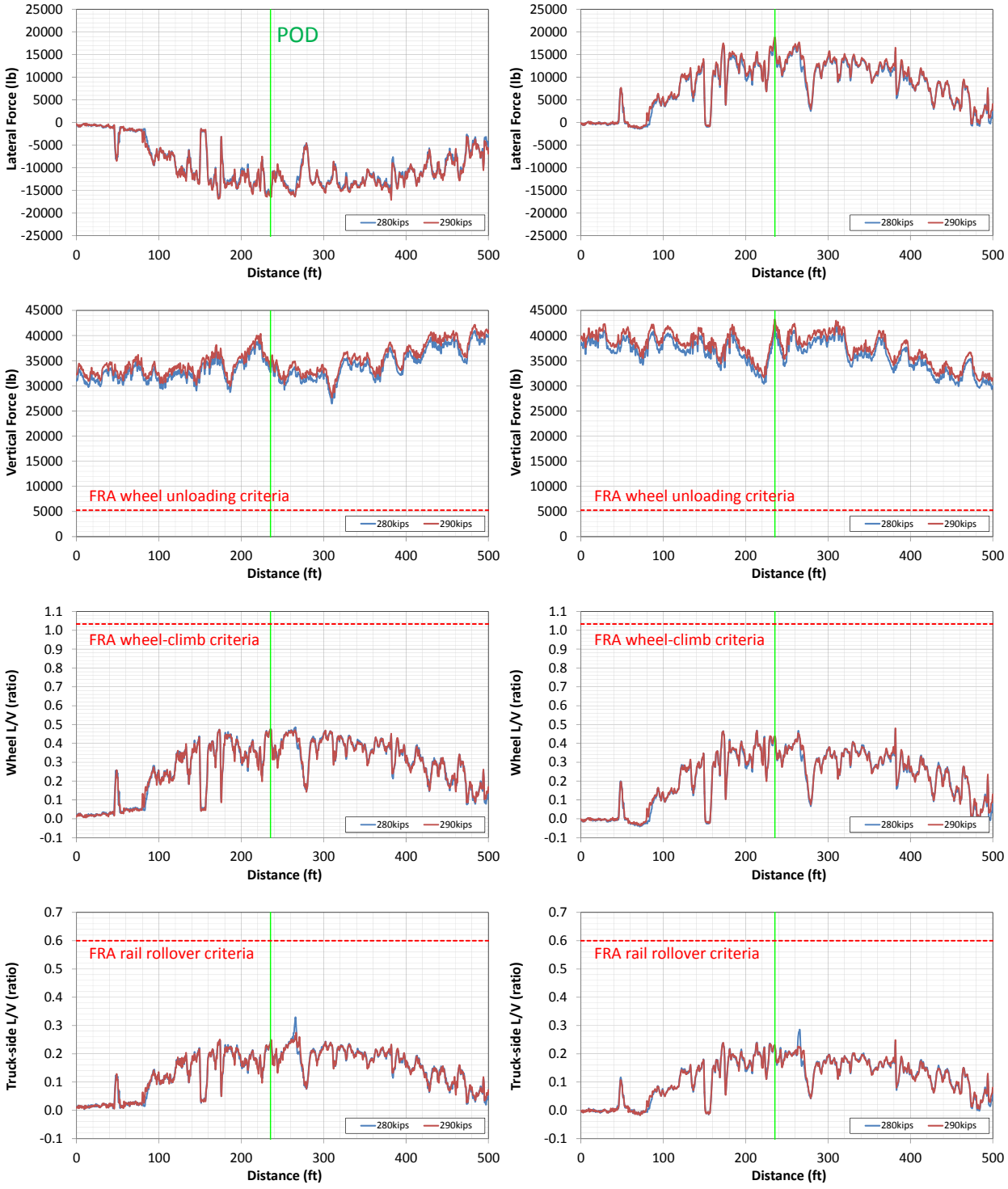

Figure C1: Axle 1 predicted wheel-rail forces in derailment curve, effect of carbody weight: comparison of baseline case car with weight of 280 kips and car weight of 290 kips, center of gravity of 93 inches.

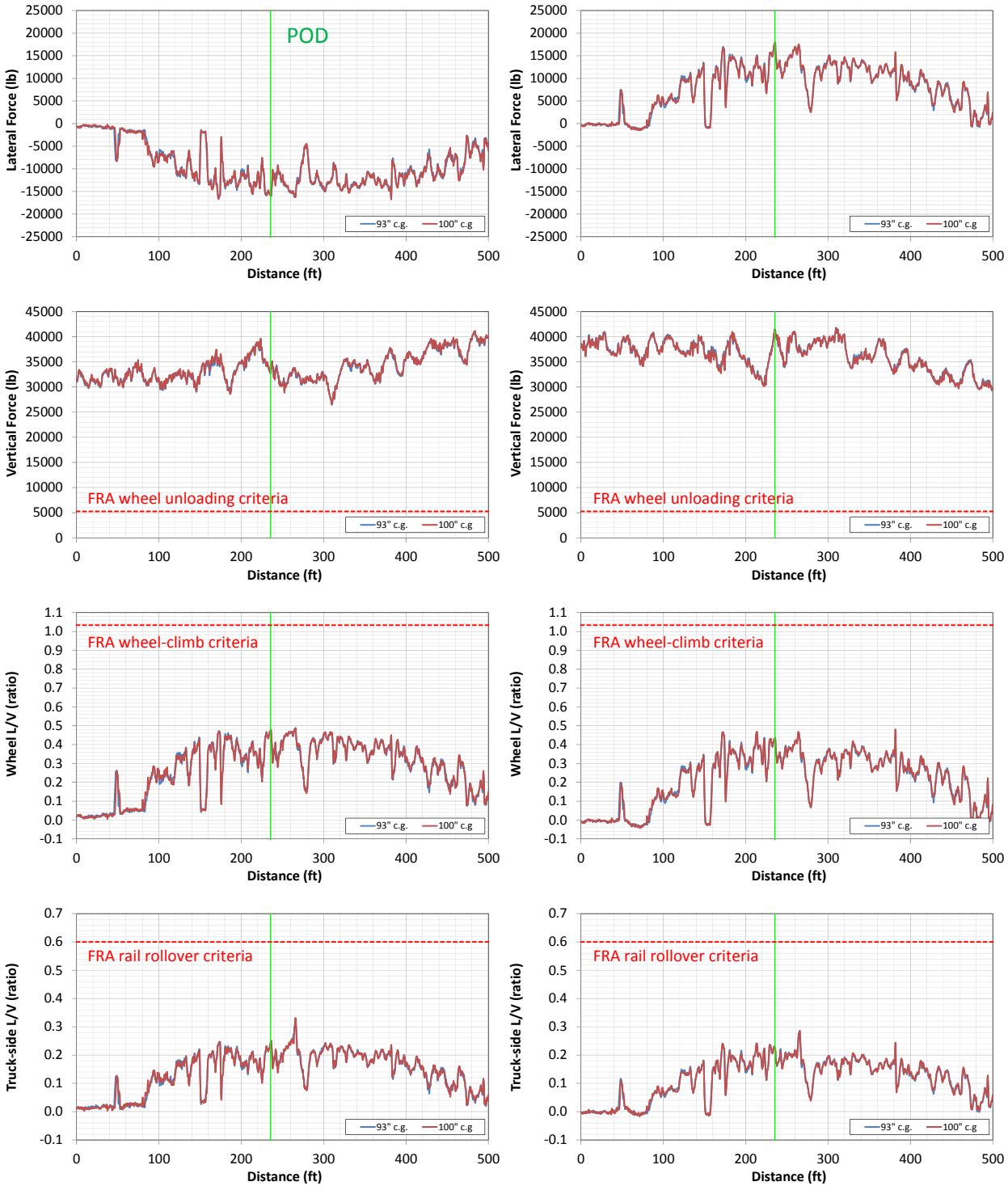

Figure C2: Axle 1 predicted wheel-rail forces in derailment curve, effect of center of gravity: comparison of baseline car with center of gravity of 93 inches and car center of gravity of 100 inches, weight of 280 kips.

APPENDIX D – RAIL CANT AND LOADED GAGE DUE TO RAIL SEAT DEFLECTION OF CENTER-BOUND CROSSTIE

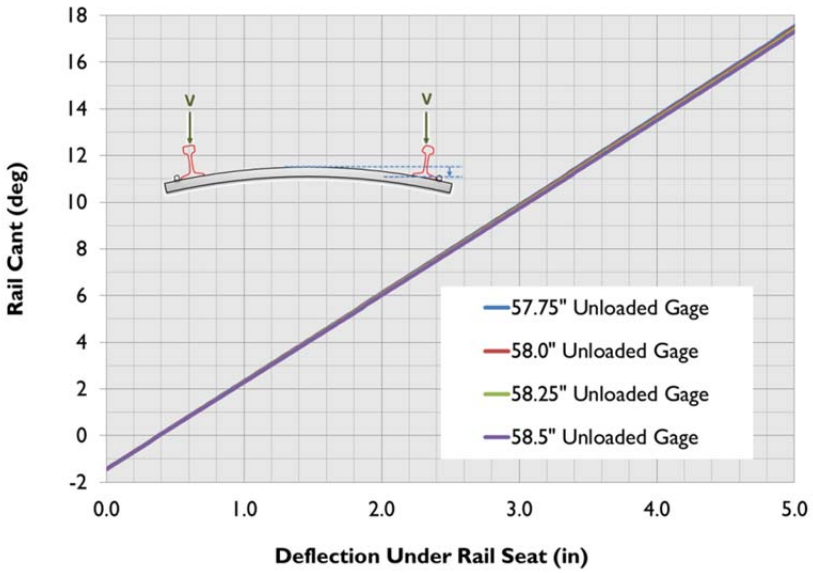

Figure D1: Rail cant for a given crosstie deflection – single center-bound crosstie.

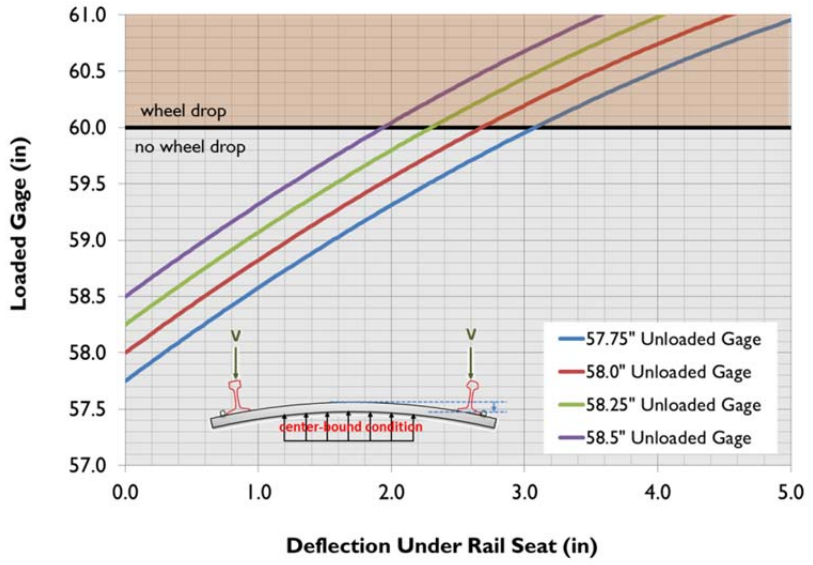

Figure D2: Loaded gage for given crosstie deflection –center-bound crosstie.

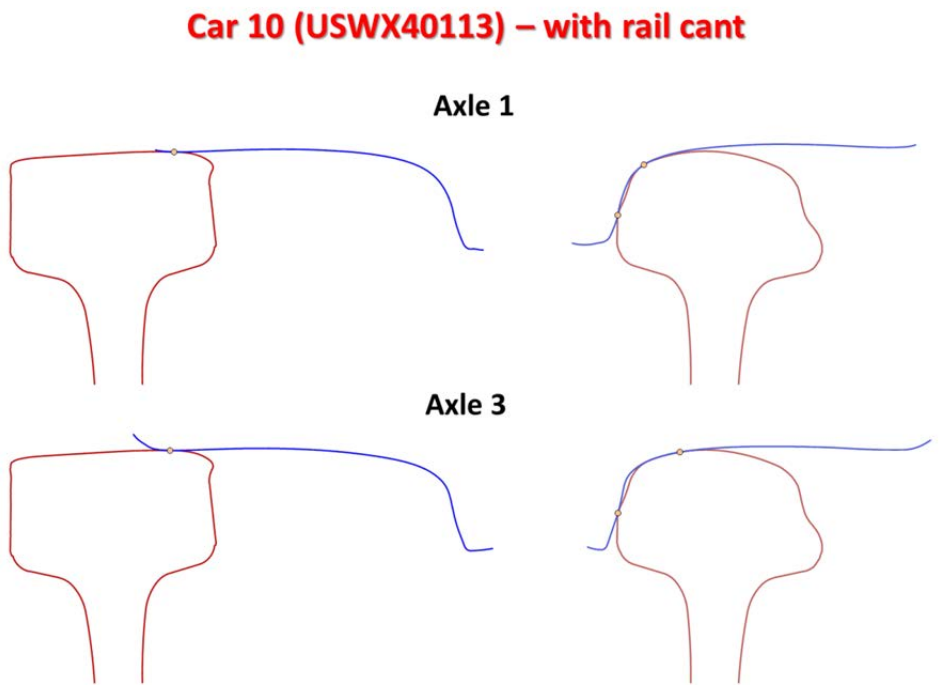

Figure D3: Wheel-rail contact geometry for car 10 axles 1 and 3 (lead truck axles) on canted rails.

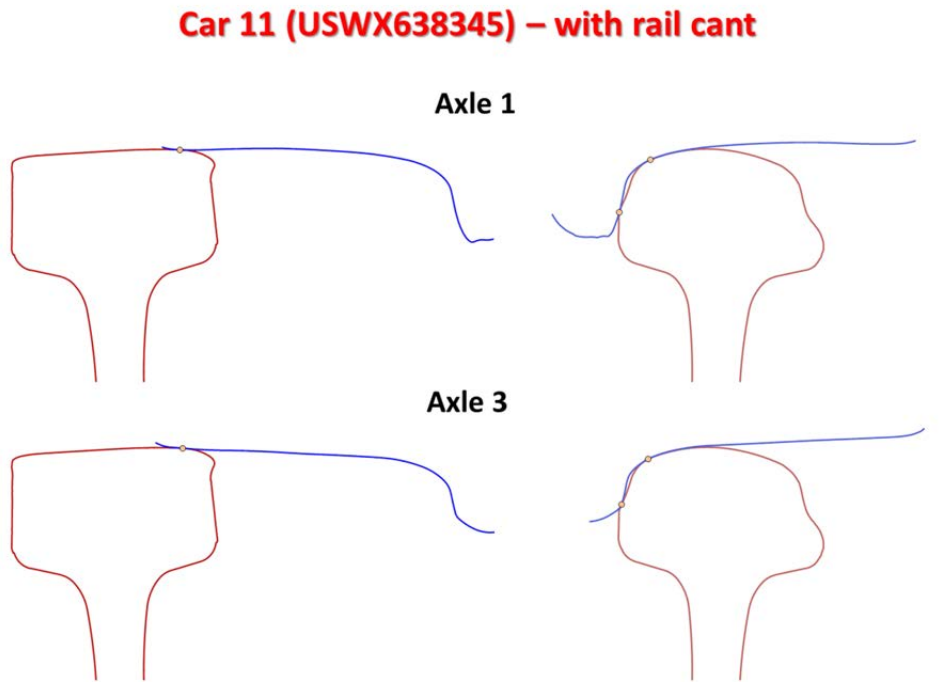

Figure D4: Wheel-rail contact geometry for car 11 axles 1 and 3 (lead truck axles) on canted rails.

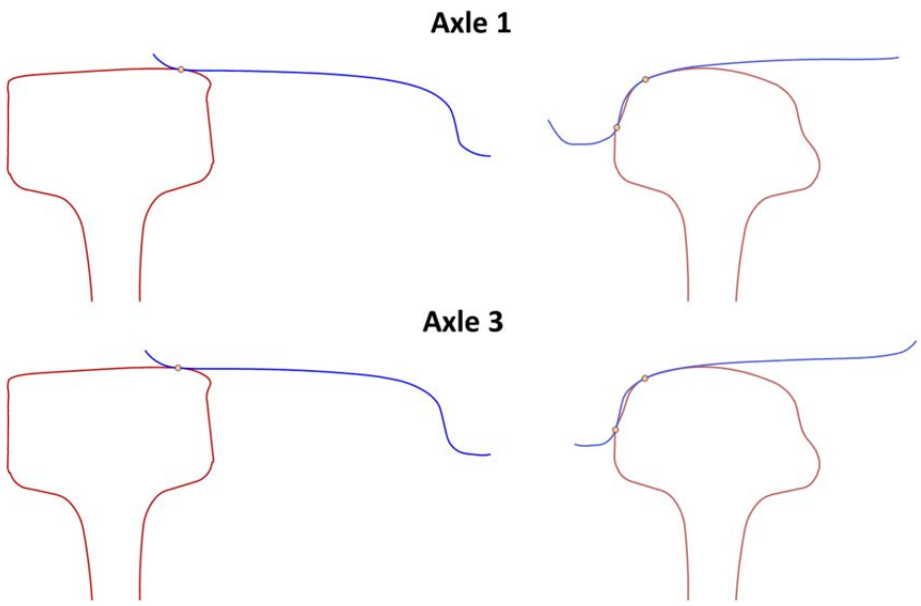

Figure D5: Wheel-rail contact geometry for car 12 axles 1 and 3 (lead truck axles) on canted rails.